AFOSR-TR-97 971

0533

REPORT DOCUMENTATION PAGE

OMB No. 0704-0188

1. AGENCY USE ONLY (Leave blank)	2. REPORT DATE	3. REPORT TYPE AND DATES COVERED
	09/14/97	Final Technical Report 06-15-94 06-14-97

4. TITLE AND SUBTITLE
Aerodynamic Flow Vectoring of Wakes and Jets for High Lift Control

5. FUNDING NUMBERS
F49620-94-1-0358

6. AUTHORS
Dr. Larry G. Redekopp

7. PERFORMING ORGANIZATION NAME(S) AND ADDRESS(ES)
University of Southern California
Department of Aerospace Engineering
854 West 36th Place
Los Angeles, CA 90089-1191

8. PERFORMING ORGANIZATION REPORT NUMBER

9. SPONSORING/MONITORING AGENCY NAME(S) AND ADDRESS(ES)
Dr James M. McMichael
Air Force Office of Scientific Research
110 Duncan Avenue Suite B115
Bolling AFB DC 20332-0001

NA

10. SPONSORING/MONITORING AGENCY REPORT NUMBER

11. SUPPLEMENTARY NOTES

12a. DISTRIBUTION/AVAILABILITY STATEMENT
Approved for public release; distribution unlimited.

12b. DISTRIBUTION CODE

13. ABSTRACT (Maximum 200 words)

A methodology has been developed for the aerodynamic flow-vectoring control of wakes on jets. Directional flow control of wakes and jets has been demonstrated without requiring any mechnical motion of the boundaries which constrain or guide the flow. The methodology is based on global instability concepts. The key to the success of this approach is to use local suction to suppress any global instability and then exploit symmetry considerations to produce proportional directional control of this flow.

14. SUBJECT TERMS
Thrust vectoring; flow vectoring; global instability; flow control.

15. NUMBER OF PAGES

16. PRICE CODE

17. SECURITY CLASSIFICATION OF REPORT	18. SECURITY CLASSIFICATION OF THIS PAGE	19. SECURITY CLASSIFICATION OF ABSTRACT	20. LIMITATION OF ABSTRACT
Unclassified	Unclassified	Unclassified	UL

Aerodynamic Flow Vectoring of Wakes and Jets for High Lift Control

Final Report on AFOSR AASERT Grant No. F49620-94-J-0358
September, 1997

Principal Investigator: Larry G. Redekopp
Departments of Aerospace and Mechanical Engineering
University of Southern California
Los Angeles, CA 90089-1191

Office: (213) 740-5369
FAX: (213) 740-7774
e-mail: redekopp@spock.usc.edu

Flow vectoring of aerodynamic flows has long been established through the use of mechanical moving surfaces such as ailerons, elevators, flaps, etc. to redirect the local flow on an aircraft in order to obtain high-lift control or thrust vectoring. Only recently has aerodynamic flow vectoring been investigated whereby the flow may be redirected without any movable surfaces. The present study has addressed the open-loop control of a wake and a jet by means of trailing edge suction to produce aerodynamic flow vectoring.

The approach to aerodynamic flow vectoring, which was investigated under the auspices of this contract, is closely link to the existence of a global instability in wake flows. The foundational fluid mechanical problem of interest in the current study consists of the formation of the wake downstream of a bluff splitter plate by the merging or two independent streams of flow having different ambient velocities (see Figure 1). Although the wake itself has an inherent asymmetry when the two streams of fluid have different velocities, the mean flow of the unsteady wake at a supercritical Reynolds number exhibits streamlined flow aligned with the streamwise axis of the bluff splitter plate. This flow regime is characterized by the Karman vortex street, which may be referred to as a global mode, due to its large streamwise extent far beyond the near-wake region. The application of suction at the trailing edge of the bluff body serves as the control mechanism for the wake in this study. When the global mode is linearly unstable, it is only conceivable that the wake may be controlled if the control action extends far downstream of the bluff body (i.e., it must act on the "global" extent of the underlying mode). Therefore, the application of near-wake suction (or blowing) has very little influence on the directionality of the flow when vortex shedding is active. However, once sufficient suction is applied, the global instability may be suppressed and aerodynamic flow vectoring may be observed due to preferential entrainment of the boundary layers on the respective sides of the forebody immediately upstream of separation.

The effectiveness of suction as a control mechanism in the flow vectoring problem relates to its ability to reduce the size of the absolute instability region which exists in the spatially-developing flow in the near wake. Although local flow conditions may imply absolute instability, the global flowfield is destabilized only when the spatial extent of the region of absolute instability exceeds a critical size. Now, the extent of the region of absolute instability may be altered either by base blowing or base suction. We have demonstrated that base suction is preferred for vectoring purposes because it accentuates asymmetries in the near wake whereas blowing washes out asymmetries in the near wake. This is important because flow vectoring essentially involves the altering of the symmetry of an existing flow.

The degree of flow vectoring of a wake or jet flow may be expressed in terms of a flow vectoring angle. For a wake, for example, the vectoring angle may be formed by the intersection of the streamwise axis and the line form the mid-point of the base and extending through the near wake saddle point (defined for the time-averaged flow when vortex shedding is active). Once a critical suction mass flux is surpassed so that all global instabilities are suppressed, a distinct and rather abrupt turning of the near wake flow has been documented. The directionality of the flow is closely linked to the asymmetry of the uncontrolled streaming flow and the asymmetry of the applied control (suction distribution). Turning angles in excess of 20o have been realized in our simulations. Another measure of the vectoring in a flow is the lift (or, normal) force acting on the forebody when flow vectoring is realized. Some examples of the normal force coefficient for vectored wake flows shown in Figure 1 are given in Figure 2. A realization of a vectored wake flow is shown in Figure 3.

A concise summary of the flow vectoring approach we have explored for wake flows is as follows.

1. Suppression of vortex shedding (all linearly unstable global modes) is essential if local flow manipulation is to be realized.
2. Suction is an effective control for flow vectoring because it influences strongly the distribution of absolute instability in the near wake of a body.
3. The symmetry of both the base state and the applied control is important to the problem of flow vectoring.
4. Once all global instabilities have been suppressed, proportional directional control of a flow can be realized entirely by varying the symmetry properties of the suction distribution (i.e., not its strength).
5. A biased suction distribution may enhance the flow vectoring toward one side (e.g., the high-speed side) in comparison to the vectoring of the flow in the opposite direction (e.g., the low-speed side).
6. An optimization problem exists for the suction strength distribution to realize the greatest vectoring effect.

The results of the vectoring work related to wake flows has been reported in two recent publications.

- "Global dynamics of symmetric and asymmetric wakes," ***J. Fluid Mech.***, 331, 231-260 (1997).
- "Global dynamics and aerodynamic flow vectoring of wakes," ***J. Fluid Mech.***, 338, 231-248 (1997).

The results and experience gained from the wake vectoring study has been extended to the case of co-flowing, two-dimensional jets. The approach is a straightforward extension of the wake vectoring problem in that we consider a jet formed as a high-speed flow exits past blunt-based jet lips. The jet is then vectored by applying suction control to the individual wakes behind each jet lip. The approach has been shown to be reasonably effective in that lift-to-thrust ratios of up to 20% have been achieved for suction volume fluxes of 6% of the jet flow. An example is shown in Figure 4. A manuscript reporting the results of this work relating to jet-vectoring is underway.

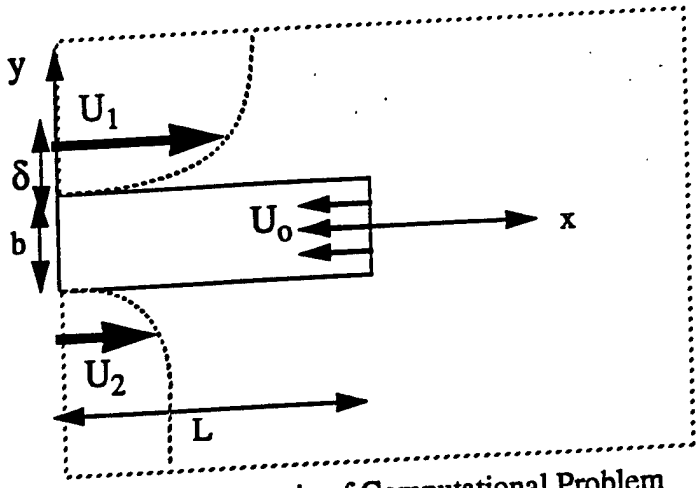

Figure 1. Schematic of Computational Problem

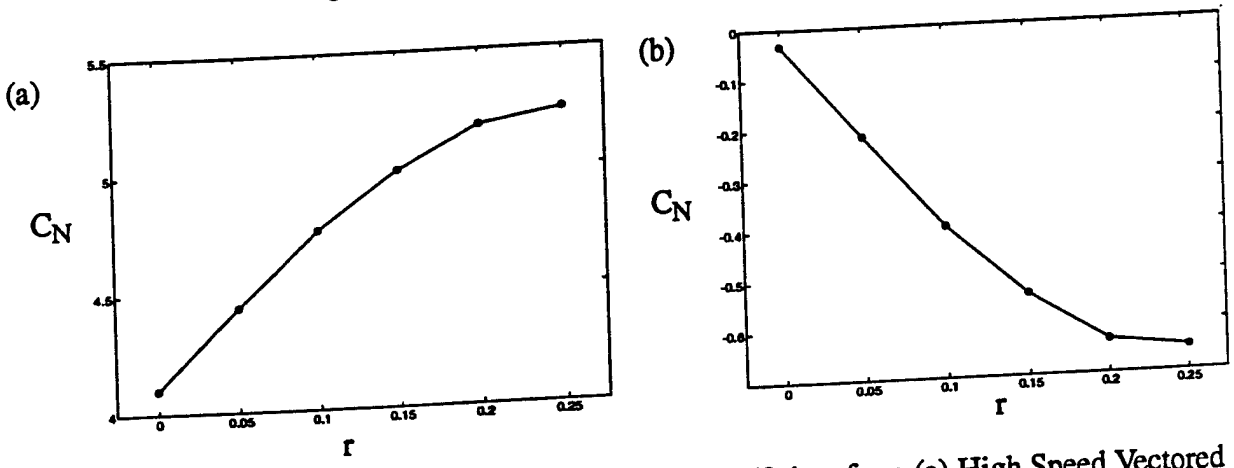

Figure 2. Effect of Shear on Normal Force Coefficient for a (a) High Speed Vectored Flow and a (b) Low Speed Vectored Flow Subject to Uniform Suction (Re=320, δ=1.2)

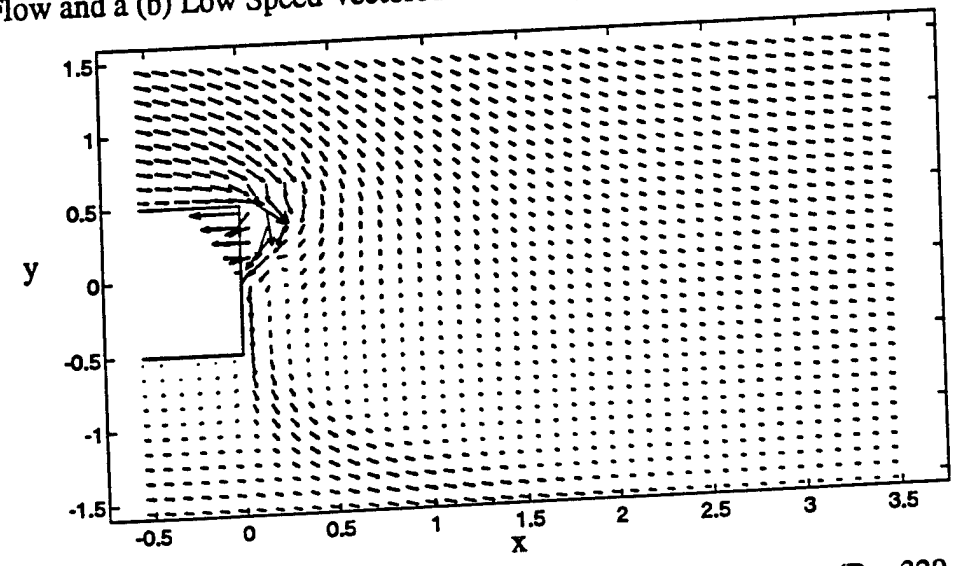

Figure 3. Vector Velocity Field of a High Speed Vectored Flow (Re=320, r=0.2, δ=1.2)

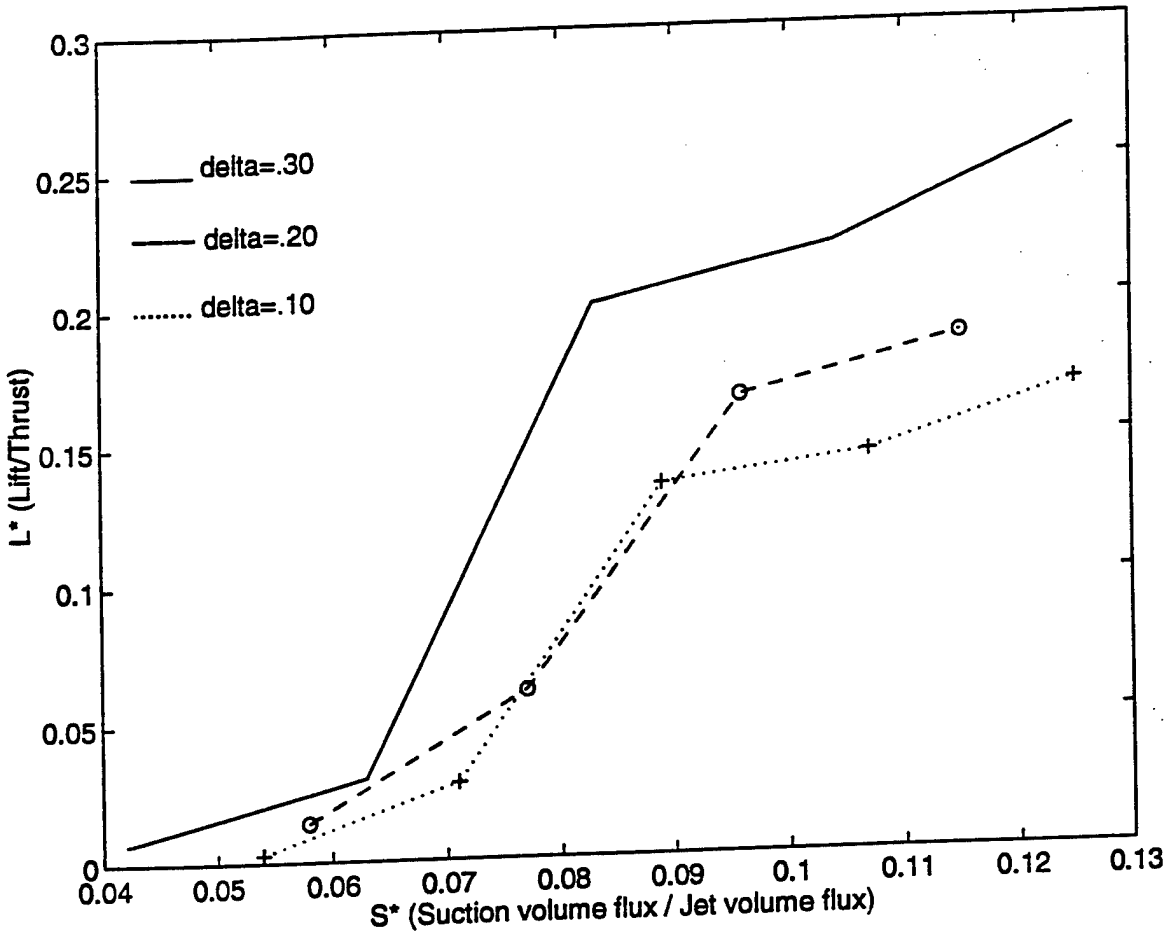

Figure 4. Lift-to-thrust ratio for a 2-D jet versus the applied suction control flux.

J. Fluid Mech. (1997), vol. 331, pp. 231–260

Global dynamics of symmetric and asymmetric wakes

By D. A. HAMMOND AND L. G. REDEKOPP

Department of Aerospace Engineering, University of Southern California, Los Angeles, CA 90089-1191, USA

(Received 30 May 1995 and in revised form 22 February 1996)

The two-dimensional wake–shear layer forming behind a rectangular-based forebody with independent ambient streams on either side of the forebody is examined by direct numerical simulation. Theoretical aspects of global modes and frequency selection criteria based on local and global stability arguments are tested by computing local stability properties using local, time-averaged velocity profiles obtained from the numerical simulations and making the parallel-flow approximation. The theoretical results based on the assumption of a slightly non-parallel, spatially developing flow are shown to provide a firm basis for the frequency selection of vortex shedding and for defining the conditions for its onset. Distributed suction or blowing applied at the base of the forebody is used as a means of wake flow modification. The critical suction velocity to suppress vortex shedding is calculated. It is shown that local directional control (i.e. vectoring) of the near-wake flow is possible, but only when all global modes are suppressed.

1. Introduction

The spatio–temporal dynamics of bluff-body wake flows has been clarified considerably in recent years. These advances have been realized through a variety of approaches including stability analyses, model studies, experiments and numerical simulations. One of the key concepts emerging from these different approaches, and one which has been particularly revealing, is that of a global mode which underlies the streamwise structure of the wake and its discrete frequency selection. The important concepts and discussions of the applicability of global modes to general flows, including wakes, are presented in the reviews by Huerre & Monkewitz (1990) and Monkewitz (1993). A principal motivation behind the present study is to test some of the detailed aspects of theoretical predictions concerning the destabilization and nonlinear structure of global modes by means of an interactive combination of numerical simulation and stability analysis. At the same time, the study is designed to explore some resulting ideas related to control and symmetry breaking in a spatially developing, quasi-parallel shear flow.

Bluff-body wakes are typical of a class of shear flows where local, time-averaged velocity profiles may undergo changes in the nature of the local instability at different spatial positions along the path of its streamwise development. In the near-wake region, where there is a large velocity deficit in local cross-stream profiles of mean velocity, the local flow is typically absolutely unstable: a band of instability waves exists with group velocities directed both upstream and downstream. In the far-wake region, where the velocity deficit is much smaller, the local flow is almost

always convectively unstable: the entire band of unstable wavenumbers propagates in the downstream direction. These properties have been clearly established by stability analyses of measured and model wake profiles (cf. Mattingly & Criminale 1972; Koch 1985; Triantafyllou, Triantafyllou & Chryssostomidis 1986; Triantafyllou, Kupfer & Bers 1987; Monkewitz 1988; and Hannemann & Oertel 1989).

The implications of such spatially varying stability properties for the global dynamics of a flow were subsequently examined theoretically and numerically using a model equation possessing generic, but spatially inhomogeneous, dispersive properties. In particular, Chomaz, Huerre & Redekopp (1988, 1991) demonstrated that flows of mixed stability type over their streamwise development can exhibit an internal resonance when a spatial region of absolute instability of 'sufficient size' is sandwiched within contiguous regions of convective instability. The resonance is self-excited and characterized by a sharp frequency selection. The onset of these spontaneous dynamics, which is analogous to that of wake flows as the Reynolds number exceeds the critical value for vortex shedding, occurs via a Hopf bifurcation. This latter fact was verified experimentally in wakes behind cylinders by Mathis, Provansal & Boyer (1984), Provansal, Mathis & Boyer (1987) and Sreenivasan, Strykowski & Olinger (1986). Some of the dynamical characteristics described above, together with some of the links to underlying stability properties, have also been observed in numerical simulations (cf. Triantafyllou *et al.* 1986; Zebib 1987; Hannemann & Oertel 1989; and Karniadakis & Triantafyllou 1989, 1992). More recently Schumm, Berger & Monkewitz (1994) have provided detailed experimental measurements in wakes behind several different bluff bodies further validating the applicability of a Stuart–Landau model for the onset of vortex shedding and the nature of the bifurcated state, together with its response to various control inputs.

The spatial structure of the post-bifurcation state (e.g. that of active vortex shedding) exhibits organized dynamics over streamwise length scales which are large in comparison to the streamwise scale of the pocket of absolute instability responsible for the appearance of the state. This dynamical state is termed a *global mode* since it is describable in terms of a *streamwise* eigenmode which is destabilized when a control parameter (e.g. the Reynolds number) exceeds a critical value. This critical value of the control parameter for global instability is typically considerably greater than the value of the control parameter for which local instability would be possible on a parallel flow basis. The global mode is damped in the pre-bifurcation state and it is spontaneously excited in the post-bifurcation state. It is worth noting that any observed global mode state is, in fact, a nonlinear entity since some self-limiting nonlinearity is required to achieve a realizable equilibrium state.

The important link between local instability properties and global dynamics in flows exhibiting internal, spontaneous resonances has been established theoretically via a slowly varying or WKBJ approach (cf. Chomaz *et al.* 1991; Monkewitz, Huerre & Chomaz 1993 and Le Dizès *et al.* 1996). This intimate, but powerful, link between local and global states is both appealing and useful for understanding the observed dynamics and for proposing scenarios, or the lack thereof, for flow manipulation. For example, the theory identifies a specific spatial position in the absolutely unstable region where an effective 'wave-maker' is positioned, providing a precise frequency selection criterion for the global mode at the bifurcation point. It also reveals the existence of some type of integral criterion for the initial destabilization of a global mode and provides some important insights pertaining to the forcing of these modes (cf. Chomaz, Huerre & Redekopp 1990). However, in many real flows the assumptions underlying the WKBJ approach are not approximated very closely. For

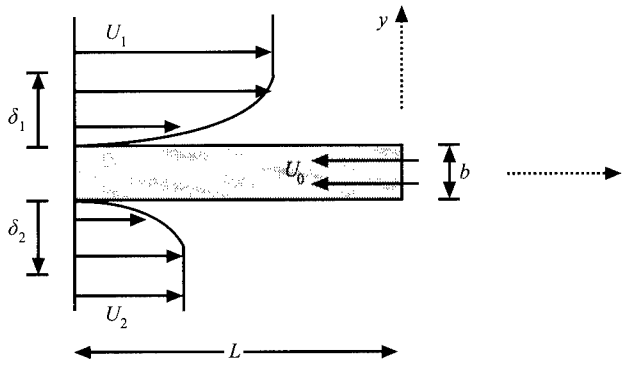

FIGURE 1. Flow configuration.

example, the spatially developing wake flow at conditions only slightly below the critical Reynolds number for onset of vortex shedding has local velocity profiles which are clearly unstable based on a parallel-flow approximation. Nevertheless, the pre-bifurcation state does not display any noise amplification of existing convective or absolute instabilities, evidently, because the spatial non-uniformity of the flow is so strong. Hence, there are two effects characterizing the wake at subcritical conditions: the strong spatial non-uniformity of the flow and the under-developed region of local absolute instability. Since vortex shedding is a global dynamical state and the marginally stable, subcritical state has locally unstable profiles, it seems clear that the streamwise non-uniformity of wake flows and their spatially varying stability properties are important features underlying the observed spatio–temporal dynamics of this class of free shear flows. Consequently there is a need to validate some of the theoretical predictions for global modes and to examine the robustness of these predictions in contexts where the underlying theoretical assumptions are violated. This forms the principal motivation for the present study. The results of the study reveal the utility of the theoretically established concepts and criteria.

2. Problem formulation

The general flow configuration studied here consists of two independent streams of incompressible fluid flowing parallel to each other on opposite sides of a (semi-infinite) body with a rectangular base. A wake forms downstream of the fixed separation points of the rectangular base. A sketch of the flow configuration is provided in figure 1. The ambient speeds of the two streams are specified independently so a persistent shear can be imposed across the developing wake. The base height b is used as the length scale and the average velocity U_∞ of the two streams is used as the reference velocity. With these scales, the relevant dimensionless parameters are the Reynolds number Re and the velocity ratio r defined as

$$Re = \frac{U_\infty b}{\nu}, \qquad r = \tfrac{1}{2}(U_1 - U_2). \tag{2.1}$$

Note that U_1 and U_2 are dimensionless stream speeds scaled with the dimensional velocity U_∞. The computational domain (nominally) extends from three units (i.e. a length equal to $3b$) upstream of the rectangular base of the forebody to 20 units

downstream. Convective outflow boundary conditions

$$\frac{\partial \boldsymbol{v}}{\partial t} + u(x_e, y, t)\frac{\partial \boldsymbol{v}}{\partial x} = 0, \tag{2.2}$$

where $\boldsymbol{v}$ is the velocity, are applied at the position x_e at the downstream end of the computational domain. The inlet flow is specified, on respective sides of the forebody, to consist of ambient streams with uniform streamwise velocities U_1 and U_2 contiguous with (nominally Blasius) boundary layers of thicknesses δ_1 and δ_2 adjacent to the parallel walls of the forebody. The lateral boundaries of the computational domain extend approximately 20 units on each side from the walls of the forebody. Along these boundaries the streamwise velocity is set equal to the respective ambient value and the perturbation pressure is supposed to vanish. The cross-stream velocity on these lateral boundaries is unspecified so that some weak inflow or outflow along these permeable boundaries is allowed. The no-slip conditions are applied along the walls of the forebody and the velocity vector is specified on the base so that arbitrary spatial distributions and angles of blowing or suction can be imposed as a means of wake flow modification. In what follows we suppose the dimensionless velocity U_0 is positive for base suction as shown in figure 1.

The direct numerical simulation of the two-dimensional, unsteady Navier–Stokes equations in primitive variables for an incompressible fluid was based on the QUICKEST (Quadratic Upwind Interpolation for Convective Kinetics with Estimated Streaming Terms) scheme proposed by Leonard (1979) and adapted by Davis & Moore (1982) and Davis, Moore & Purtell (1984). This finite-difference scheme was chosen because of its simplicity of implementation and it is easy to incorporate more complex geometric configurations like tandem wakes and two-dimensional jets. The production version of the code employed in the study presented here used a two-level grid. A uniform grid with $\Delta x = \Delta y = 0.1$ was used in the central streamwise strip extending from the edge of one boundary layer to the other boundary layer. In the regions external to this strip, the grid in the cross-stream direction was stretched by a factor of 8% per interval as one proceeds away from the wake. This is illustrated in figure 2.

The numerical simulation was validated by comparing the computed frequency of vortex shedding for symmetric flow (i.e. $r = 0$) with the numerical results reported by Hannemann & Oertel (1989). They studied the same flow, albeit with slightly different boundary layer in-flow. Using a Reynolds number of 200 and fixing the boundary layer thicknesses to be approximately equal to the values corresponding to their case, the shedding frequency (or Strouhal number when non-dimensionalized with the average velocity U_∞ and base height b) agreed to within 10% using the nominal grid defined above. Refinement of the grid by a factor of 2 resulted in only a 1% change in the shedding frequency. Another measure of the computational accuracy is to evaluate the degree to which mass is conserved. For simulations using the nominal grid, a global mass loss of 0.01% was found over a time period of 10 vortex-shedding periods. Tests were also made to evaluate the effect of the downstream boundary conditions, or the location where these conditions were applied. To this end, simulations were made for a symmetric wake ($r = 0$) in the absence of suction ($U_0 = 0$) at $Re = 320$ and with inlet boundary layer thicknesses of $\delta_1 = \delta_2 = 1.2$ where the downstream end of the computational domain was varied from 20 to 37 to 97 units from the base of the forebody. The shedding frequency was measured along with the amplitude (i.e. one-half the peak-to-peak value) of the velocity fluctuations (Δu_s, Δv_s) of the saturated shedding state at the fixed point ($x = 1$, $y = 1/2$) in the wake. The results are given in table 1. The

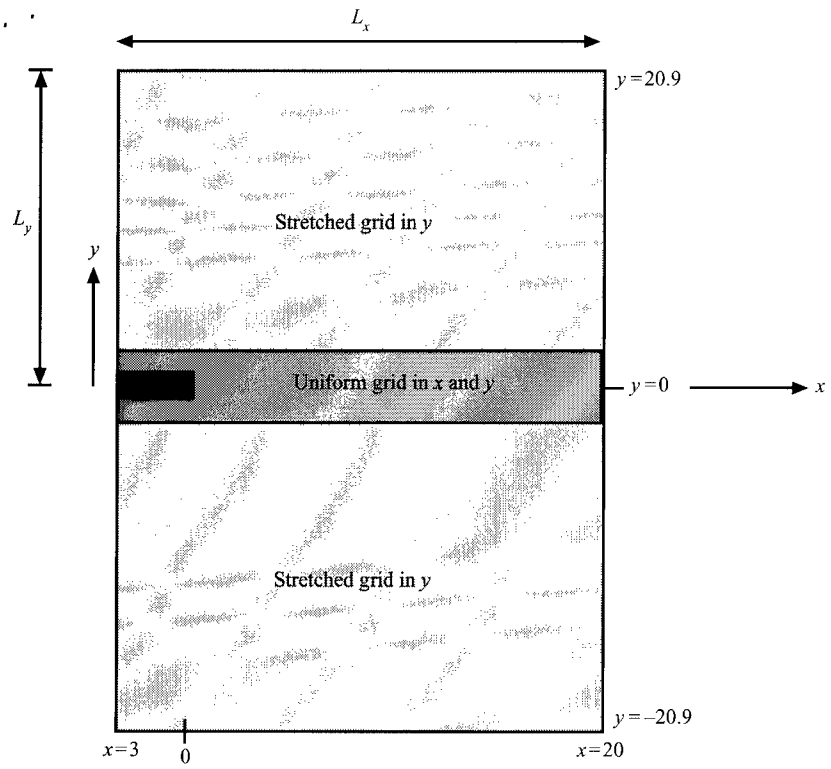

FIGURE 2. Computational domain with two-level grid.

	$-3 < x < 20$ $nx = 230$	$-3 < x < 37$ $nx = 400$	$-3 < x < 97$ $nx = 1000$
f	0.1065	0.1087	0.1086
Δu_s	0.0626	0.0626	0.0630
Δv_s	0.0725	0.0802	0.0807

TABLE 1. Results from a test of the position of the downstream boundary conditions.

shedding frequency increased by about 2% when the domain was extended from the nominal position of 20 units downstream. The amplitude of the streamwise velocity fluctuation was essentially constant while the amplitude of the transverse velocity fluctuation increased by about 10% in the extended domain. These results provided a basis for confidence in the code and the selected grid parameters. The shorter computational domain was used because the available computational resources were limited.

3. Global mode dynamics in a symmetric wake

Simulations for symmetric wake flows ($r = 0$) were performed to provide data sets which could be analysed for both their global dynamics and local stability properties. Simulations were performed for different Reynolds numbers in the absence of any base bleed or suction and with an inlet boundary layer thickness of $\delta = 1.2$ on each

side. The boundary layer thickness was chosen to be comparable to that used by Hannemann & Oertel (1989) and was not varied for the simulations described in this paper. If the boundary layer thickness is reduced much further, a refinement in the grid is required which in turn requires greater computational resources. The displacement thickness of the boundary layers for this choice of δ was computed to be $\delta^* = 0.396$ at one grid point upstream of separation and $Re = 160$. It varied only slightly (about 1%) over the Reynolds number range considered here. Ideally, the Reynolds number at separation should be based on the geometric base height plus the displacement thicknesses of the boundary layers, but we have chosen to always quote the Reynolds number as defined in (2.1) and as it would appear in the scaled equations of motion.

We present first results of a simulation performed at a slightly supercritical Reynolds number, $Re = 160$, which was used most comprehensively to make comparisons with theoretical predictions. Time series of the streamwise velocity and corresponding frequency spectra for the saturated vortex-shedding state obtained at different spatial positions in the wake are shown in figure 3. There is clearly a single fundamental frequency (i.e. Strouhal number) $f = 0.1$ that is uniform throughout the wake. The existence of a global frequency had been established in early studies by Kovasznay (1949) and Roshko (1954). However, some confusion arose after Tritton (1959) reported the existence of two frequencies in a cylinder wake when the Reynolds number was in a certain range. This was clarified by Williamson (1988, 1989) who showed that the double-frequency measurements were stimulated by end effects which could induce oblique vortex shedding across the entire span. Model studies by Albarède & Monkewitz (1992) and Park & Redekopp (1992) have shown that these three-dimensional effects can be understood in terms of spanwise-propagating phase modes. Williamson shows that, when end effects are eliminated, the wake remains two-dimensional with a single, global frequency for $Re < 180$ in cylinder wakes. This corresponds to a supercriticality parameter

$$\Delta = \frac{Re - Re_{cr}}{Re_{cr}} \tag{3.1}$$

of $\Delta \simeq 2.83$ assuming a value of $Re_{cr} = 47$. Computations by Karniadakis & Triantafyllou (1992) suggest that three-dimensional effects appear for $200 < Re < 210$, or $3.26 < \Delta < 3.47$, in cylinder wakes. In the present study we estimate $Re_{cr} \simeq 120$, which yields $\Delta = 0.33$ for the simulation at $Re = 160$ shown in figure 3. Furthermore, the highest Reynolds number considered is 520 corresponding to $\Delta = 3.33$.

Mean velocity profiles at various streamwise positions were computed for the saturated state in order to establish connections between local stability properties and global dynamics. The wavenumber k_{max} corresponding to the most amplified temporal instability mode at each streamwise station was computed using an Orr–Sommerfeld solver with $Re = 160$. This wavelength λ_{max} was compared with the length scale L for variation of the momentum thickness θ of the wake in order to obtain a measure of the non-parallel nature of the spatially developing flow in terms of the parameter

$$\epsilon = \frac{1}{k_{max}} \left(\frac{1}{\theta} \frac{\mathrm{d}\theta}{\mathrm{d}x} \right) = \frac{\lambda_{max}}{L}. \tag{3.2}$$

The variation of ϵ with the streamwise distance is shown in figure 4. It is clear that streamwise gradients in the developing mean flow are not necessarily small for, say, $x < 6$. Consequently, direct quantitative comparisons between the present results and asymptotic theories should not be expected to yield good correspondence.

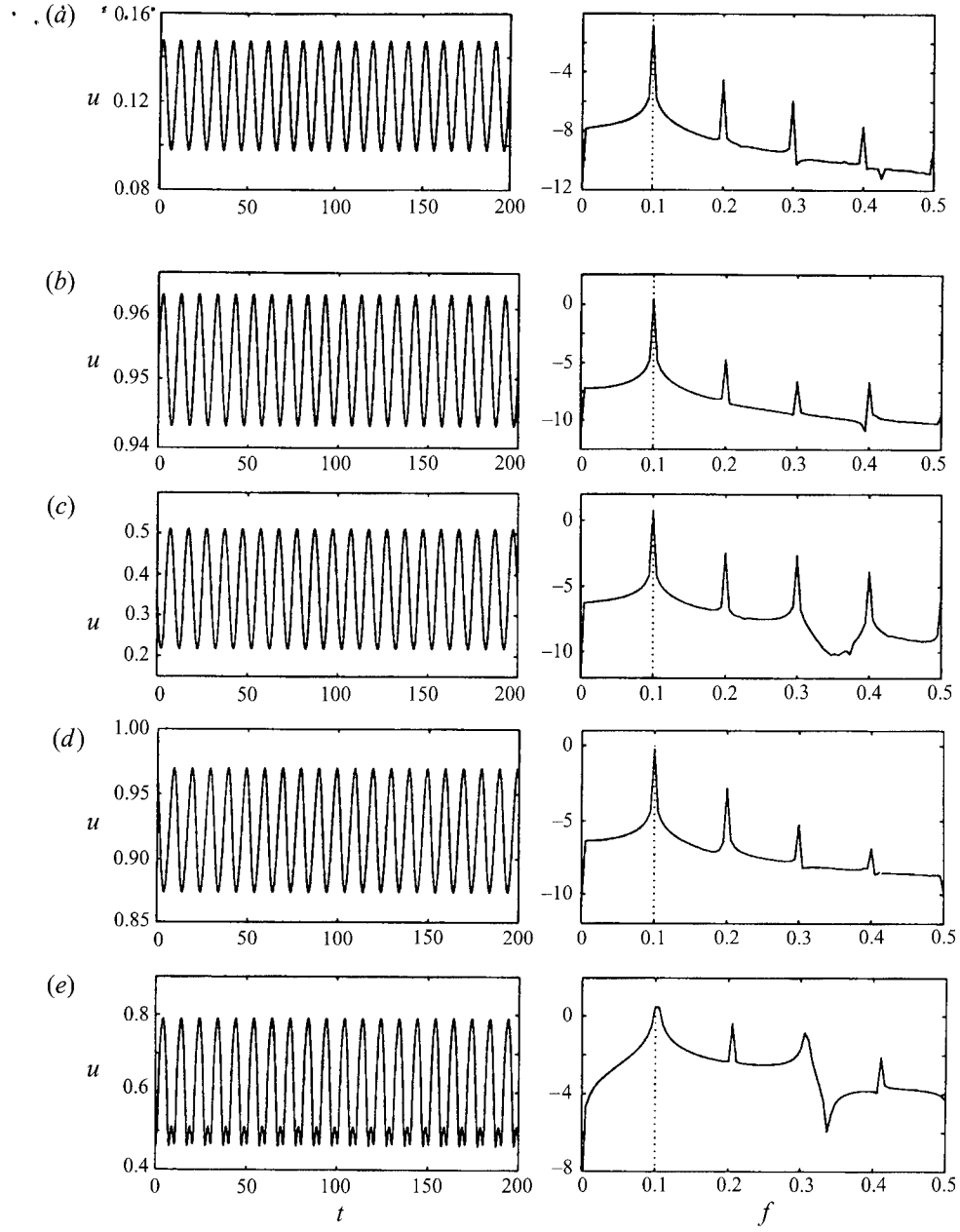

FIGURE 3. Time series and corresponding frequency spectra for the saturated wake at $Re = 160$ at different spacial locations: (*a*) $x = 1, y = 1.45$; (*b*) $x = 1, y = 1.45$; (*c*) $x = 5, y = 0.45$; (*d*) $x = 5, y = 1.45$; (*e*) $x = 10, y = 0.45$.

Frequency wavenumber pairs (ω_0, k_0) corresponding to the sinuous mode with vanishing group velocity (i.e. $\partial\omega/\partial k = 0$) were computed based on a locally parallel stability analysis of the mean velocity profiles at different streamwise positions. The results for $Re = 160$ are shown in figure 5. It is evident from the plot of the absolute growth rate $\omega_{0i}(x)$ that the wake is locally absolutely unstable for $0 < x < 3.15$. The global mode for this case, however, extends far beyond the point $x_{AU} = 3.15$.

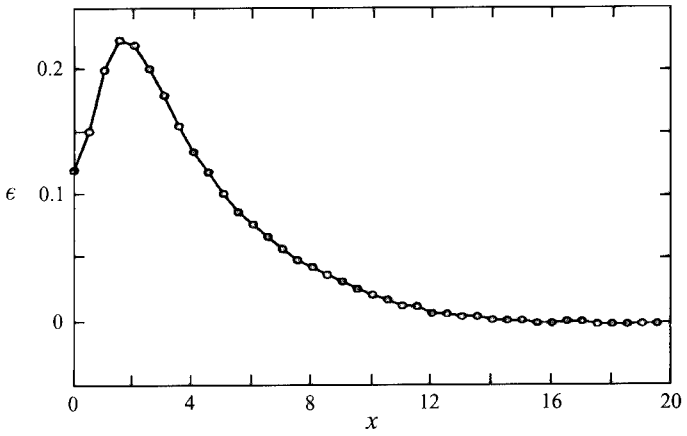

FIGURE 4. A measure of the non-parallel nature of the spatially developing wake at $Re = 160$.

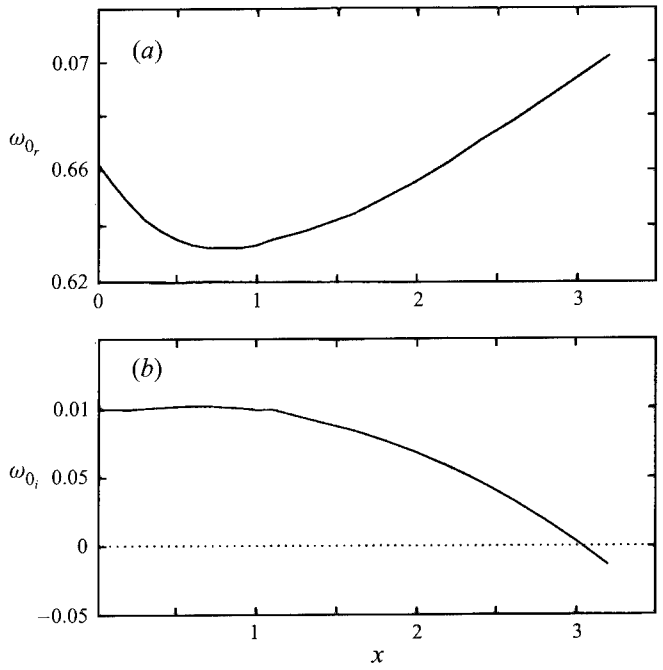

FIGURE 5. (*a*) The absolute frequency and (*b*) the absolute growth rate for the wake at $Re = 160$.

A representation of the global mode is shown in figure 6 where the transverse velocity along the wake centreline is plotted for four equally spaced phases of the vortex shedding cycle in the saturated state. For the purpose of computing the global mode in the present problem, the computational domain was extended to 100 base heights downstream of the forebody. However, as seen from figure 6, the global mode extends beyond the computational domain and encompasses a streamwise scale which is more than 30 times the length of the absolutely unstable pocket. By way of comparison, Kovasznay (1949) and Eisenlohr & Eckelmann (1988) suggest that the Kármán vortex street behind a cylinder extends (roughly) to 30 diameters downstream for Reynolds number not too far above the critical value. We point

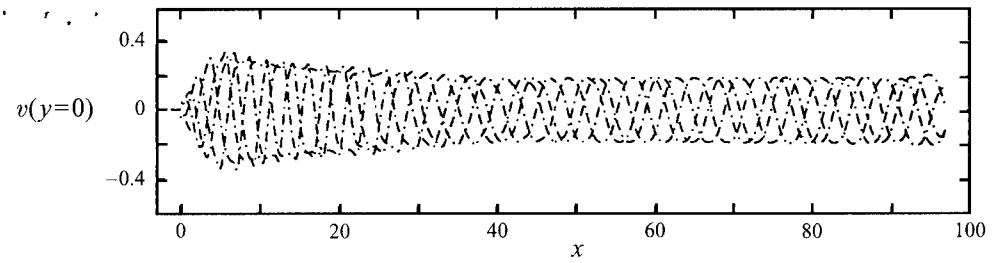

FIGURE 6. The global mode structure in the wake at $Re = 320$.

out, parenthetically, that the results of figure 6 provide an excellent validation of the outflow boundary conditions. They are found to have no distinguishable effect on the structure of the global mode. In fact, the results in table 1 reveal that the shedding frequency varied by less than 2% when the computational domain size was increased from 20 to nearly 100 base heights behind the body.

Criteria for the existence of global mode dynamics in a spatially developing flow, and a prediction for the selection of the frequency of the mode, were advanced by Chomaz *et al.* (1991). They showed that a finite interval Δx_{AU} of local absolute instability was a necessary condition for the existence of a global mode, and that the frequency selected by that mode was equal to the real part of the absolute frequency ω_0 evaluated at the streamwise position x_s defined by

$$\left.\frac{\partial \omega_0}{\partial x}\right|_{x=x_s} = 0. \tag{3.3}$$

Close examination of figure 5 reveals that extrema of the curves $\omega_{0_r}(x)$ and $\omega_{0_i}(x)$ occur at different streamwise positions. This is clear evidence that the saddle point x_s does not lie on the real axis. However, since derivatives of $\omega_0(x)$ are only known along the real x-axis, the location of the saddle point x_s of $\omega_0(x)$ was found through use of the Cauchy–Riemann equations and analytic continuation to complex values of $x = x_r + \mathrm{i}x_i$. This yields the expressions

$$\left.\begin{aligned} \omega_{0_r}(x_s) &= \omega_{0_r}(x_r, x_i = 0) - \left.\frac{\partial \omega_{0_i}}{\partial x_r}\right|_{x_i=0} x_i + O(x_i^2), \\ \omega_{0_i}(x_s) &= \omega_{0_i}(x_r, x_i = 0) + \left.\frac{\partial \omega_{0_r}}{\partial x_r}\right|_{x_i=0} x_i + O(x_i^2). \end{aligned}\right\} \tag{3.4}$$

Pairs of (x_r, x_i) are sought such that (3.3) is satisfied. The position of the saddle point for the symmetric wake at $Re = 160$ is $(x_{sr} = 0.79, x_{si} = 0.078)$. Straightforward application of the saddle-point criterion for the frequency selection of the global mode as computed based on local stability calculations yields the frequency $f_{sp} = (2\pi)^{-1}\omega_{0_r}(x_s) = 0.1006$. This is compared with an observed frequency in the numerical simulation (obtained from spectra shown in figure 3) of $f = 0.1000$.

The correspondence is quite surprising since the saddle-point criterion is an asymptotic result and this comparison has ignored any corrections to the global mode frequency from higher-order effects such as mean flow non-uniformity, etc. Also, the analysed state is somewhat removed from the bifurcation point ($\Delta = 0.33$) and nonlinear corrections could be significant. The close correspondence between the predicted frequency based on the saddle-point criterion and the computed value may be fortuitous in that the various corrections could be self-cancelling. In order to

quantify some of these effects, and to provide the most comprehensive comparison with the asymptotic theory, the first linear correction based on the analysis presented by Monkewitz *et al.* (1993) was computed as well. The definition of the different correction terms and how they are computed based on the numerically obtained mean-flow profiles is described in the Appendix.

Although the work by Chomaz *et al.* (1991), and more recently by Le Dizès *et al.* (1996), has shown that a necessary condition for the existence of an observable (i.e. linearly unstable) global mode is that a finite interval of locally absolutely unstable flow be present, no definitive global criterion for predicting the condition or control parameter setting for onset is available. Using several model studies of the linear Ginzburg–Landau equation, Chomaz *et al.* (1990) conjectured that destabilization of the gravest global mode and the onset of global dynamics might be described by the condition

$$I_{AU} = \int_{\Delta x_{AU}} [\omega_{0_i}(x)]^{1/2} \mathrm{d}x > M, \tag{3.5}$$

where M is some order-one constant. For the symmetric wake at $Re = 160$ shown in figures 5 and 6, $I_{AU} = 0.795$. We emphasize that this criterion does not have a rigorous asymptotic basis, but we expect that it might have some utility, especially when the absolute frequency $\omega_0(x)$ has an isolated saddle point which is not too far from the real axis. What it does imply is that the length of the absolutely unstable pocket has a more significant role than the magnitude of the absolute growth rate. As such, flow modification influencing Δx_{AU} can be expected to be especially influential in altering the conditions for onset. Of course, modifying the level of the absolute growth rate will likely accompany any modification affecting the streamwise extent of local absolute instability. Further results related to this point will be presented later.

The critical Reynolds number $Re_{cr} \simeq 120$ for the onset of vortex shedding was estimated by exploiting the established fact (see Provansal *et al.* 1987 and Sreenivasan *et al.* 1986) that vortex shedding appears spontaneously via a Hopf bifurcation. Consequently, the square of the saturation fluctuation amplitude at any point should scale linearly with the distance from the bifurcation $(Re - Re_{cr})$ (see (3.7) below). Results of this type are shown in figure 7 for the transverse and streamwise velocity components at a fixed point $(x, y) = (1.0, 0.5)$ in the wake. No attempt was made to choose the time series at the position where the global mode was a maximum in each realization (see figure 6). There may be some (possibly small) variation in the amplitude of the global mode at a fixed point that derives solely from shape changes as a function of Δ. Nevertheless, the bifurcation was supercritical and there appears to be a substantial range of parameter values where the described scaling behaviour applies. Schumm *et al.* (1994) arrived at the same conclusion based on their analysis of data from several different wake flows.

The computed dynamics can be described in terms of the Landau model for the complex amplitude of the global mode at a fixed spatial position. For this purpose, the model is written as

$$\frac{\mathrm{d}A}{\mathrm{d}t} = \sigma A - \beta |A|^2 A \tag{3.6}$$

where σ is the (complex) growth rate and β is the (complex) Landau constant. With the constraints that $\sigma_r(Re_{cr}) = 0$ and that σ_r varies linearly with distance from the

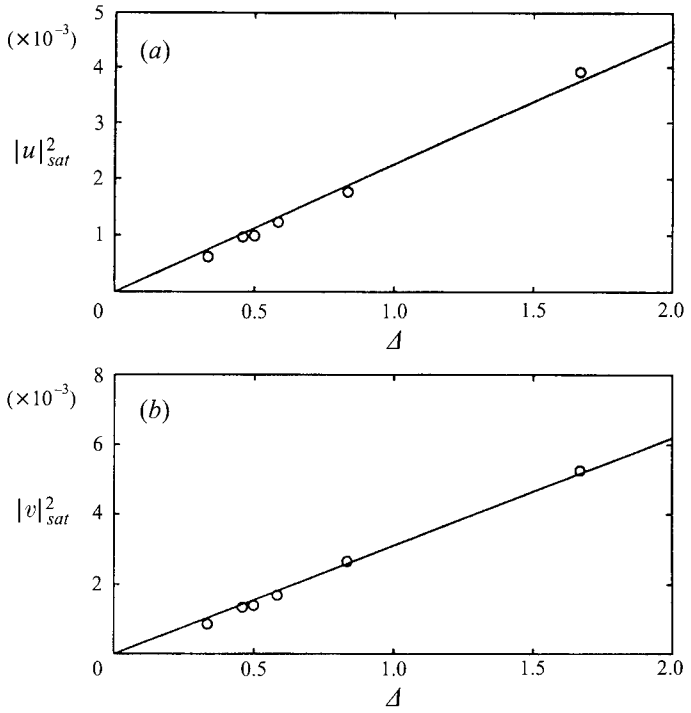

FIGURE 7. The square of the saturation amplitude of (*a*) the streamwise velocity component and (*b*) the cross-stream velocity component in the wake and its dependence on the supercriticality of the flow.

bifurcation point, one can write

$$|A|^2_{sat} = \frac{\sigma_r}{\beta_r} = \frac{1}{\beta_r}\left.\frac{\mathrm{d}\sigma_r}{\mathrm{d}\,Re}\right|_{Re_{cr}} (Re - Re_{cr}), \tag{3.7}$$

$$\frac{1}{|A|}\frac{\mathrm{d}|A|}{\mathrm{d}t} = \sigma_r\left(1 - \frac{|A|^2}{|A|^2_{sat}}\right) \tag{3.8}$$

and

$$\frac{\mathrm{d}\theta}{\mathrm{d}t} = \sigma_i - \sigma_r\frac{\beta_i}{\beta_r}\frac{|A|^2}{|A|^2_{sat}}, \tag{3.9}$$

where θ is the phase of the complex amplitude A. The temporal growth rate of the global mode was determined following the approach utilized by Schumm *et al.* (1994). Using the modulus of the streamwise velocity at a fixed spatial position ($x = 1.0$, $y = 0.5$ in this case) for a slightly supercritical Reynolds number $Re = 140$ ($\Delta = 0.167$), we obtain $(\mathrm{d}\sigma_r/\mathrm{d}\,Re)|_{Re_{cr}} = 0.0078 \pm 0.0002$ (cf. figure 8*b*). In the same way, $\sigma_i = 2\pi f = 2\pi(0.0967 \pm 0.0002)$ (cf. figure 8*c*). The difference between the linear and the saturated values of the frequency yielded the normalized Landau constant $\beta_i/\beta_r = -1.37 \pm 0.30$. These calculations were repeated at various spatial locations in the wake to verify that the 'constants' were not spatially dependent. The corrections for the respective constants quoted above encompass the variations found from the time series at different spatial positions.

A number of researchers (e.g. Sreenivasan *et al.* 1986 and Williamson 1989) have shown that there is a linear increase in the Strouhal number with Reynolds number

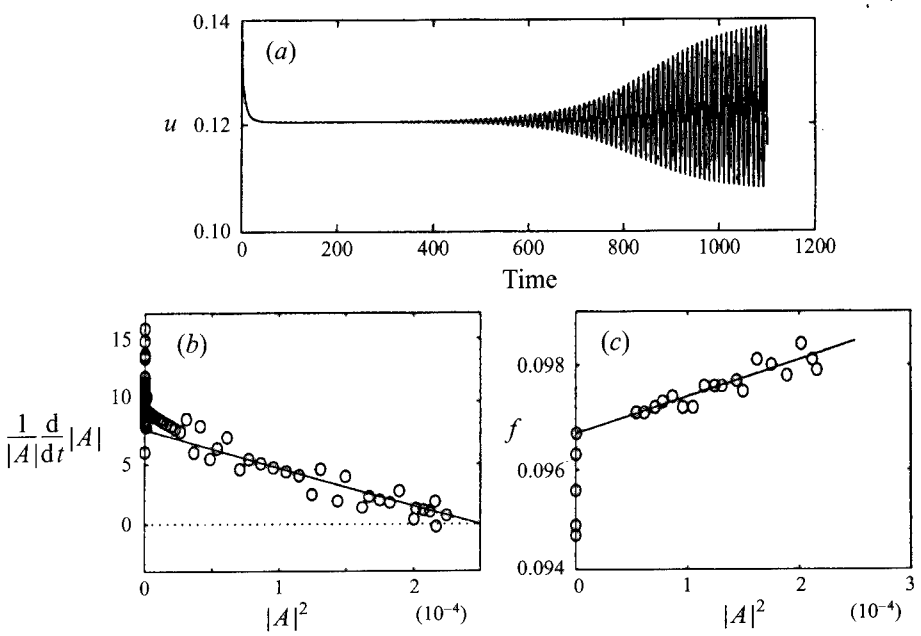

FIGURE 8. (*a*) The time series of the streamwise velocity component in the wake at $x = 1$ and $y = 0.5$ along with the corresponding temporal development of (*b*) the amplitude of the streamwise velocity component and (*c*) the vortex shedding frequency at $Re = 140$.

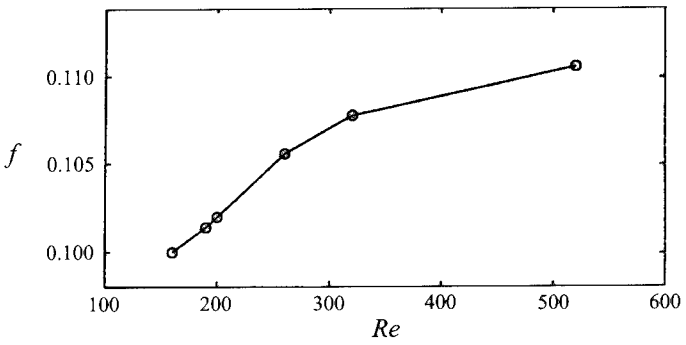

FIGURE 9. Vortex shedding frequency versus Reynolds number.

for Reynolds numbers slightly above critical. In their simulation of the symmetric wake behind a rectangular forebody similar to that studied here, Hannemann & Oertel (1989) reported a Strouhal number of 0.113 at $Re = 200$. We find a value of $f = 0.102$ at $Re = 200$, a value which is 11% smaller. However, direct comparisons should employ a Reynolds number which accounts for the displacement thicknesses of the boundary layers at separation. Since Hannemann & Oertel (1989) do not report computations of the displacement thicknesses at the trailing edge, the discrepancy in observed shedding frequency cannot be rationalized. On the other hand, Eisenlohr & Eckelmann (1988) report a universal Strouhal–Reynolds number curve for wakes behind bluff rectangular bodies which includes the displacement effect. Using a Reynolds number based on the base height plus displacement thicknesses, we obtain $f = 0.184$ compared to $f = 0.177$ (a difference of 4%) by Eisenlohr & Eckelmann (1988) at identical values of the adjusted Reynolds numbers. This provides further

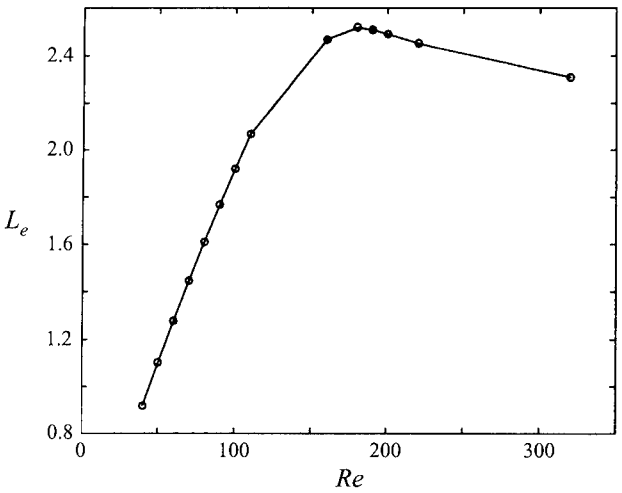

FIGURE 10. The length of the recirculation zone of the steady or time-averaged mean flow and its relation to the Reynolds number.

validation of our numerical results. The Strouhal–Reynolds number (i.e. f *vs.* Re) variation from our simulations of the symmetric wake is shown in figure 9. The Reynolds number used here excludes the displacement effect. Since the displacement thickness was (nearly) constant over the range of Reynolds numbers studied and the sum of the displacement thicknesses was 0.792 (scaled by the base height), the adjusted Reynolds number is readily obtained by multiplying by the factor 1.792.

Another measure of the symmetric wake is the streamwise distance L_e from the base of the forebody to the location of the near-wake saddle point in the streamline pattern. This is the length of the steady recirculating eddies at subcritical Reynolds numbers and the distance over which reversed flow is present in the time-average mean flow at supercritical Reynolds numbers. This length is shown in figure 10. Reference to figure 5 shows, at least for $Re = 160$, that $L_e < x_{AU}$.

4. Global mode dynamics in asymmetric wakes

One objective of this study was to investigate how the development of the wake is affected by a breaking in the symmetry of the mean flow. The measure of the symmetry of the mean flow is the velocity ratio r defined in (2.1). When r is non-zero, the flow will initially appear wake-like with a large velocity deficit. However, as the two layers of oppositely signed vorticity merge and the deficit relaxes, the flow will eventually transition from a wake flow to a shear layer flow. There is some question as to how this asymmetry will affect the structure of the global mode and how the vortex roll-up transitions from the familiar Kármán street to that of a shear layer where all vortices have the same sign. To this end, a number of simulations were performed for different velocity ratios. Throughout this study we assume that the high-speed stream is on the top ($y > 0$).

First, simulations were performed to establish the effect of mean flow asymmetry on the shedding frequency and the critical Reynolds number. Results of these simulations are shown in figures 11 and 12. The shedding frequency, at fixed Reynolds number, increases slightly with the velocity ratio. However, the critical Reynolds number decreases as the asymmetry of the ambient flow increases. The simulations shown

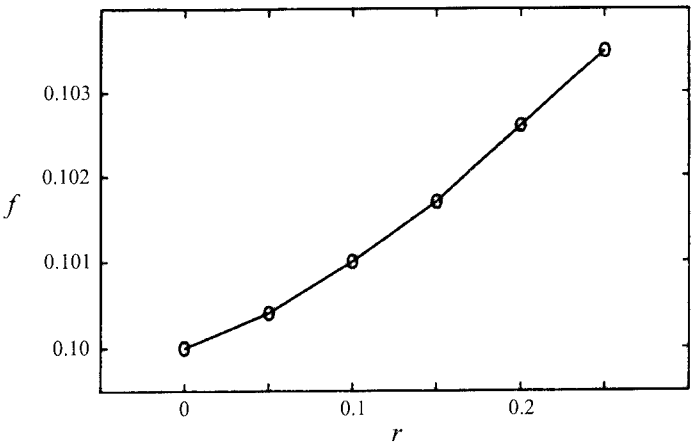

FIGURE 11. The vortex shedding frequency of the asymmetric wake at $Re = 160$.

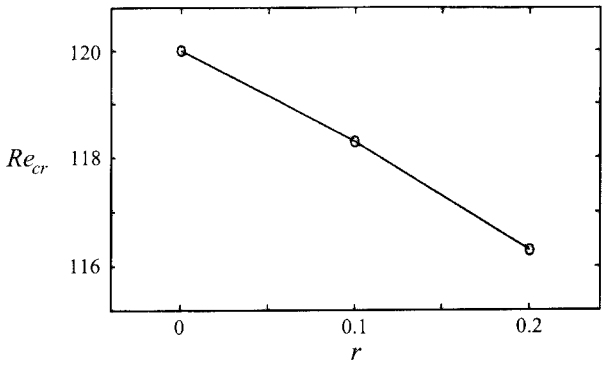

FIGURE 12. The critical Reynolds number of the asymmetric wake.

in figure 11 for $Re = 160$ were examined in more detail by taking local velocity profiles obtained from the time-averaged flow of the saturated state at each velocity ratio. The absolute frequency $\omega_0(x)$ was computed at different streamwise positions using the Orr–Sommerfeld solver together with the branch-point search algorithm. The distributions of $\omega_0(x)$, and the associated value $k_0(x)$, are presented in figure 13. Results are shown for the symmetric wake and two non-zero values of the velocity ratio. It is evident from figure 13(b) that the absolute growth rates are diminished by the effect of shear. Since these results are obtained for a fixed Reynolds number, and the critical Reynolds number decreases with increasing r, the effect of shear in decreasing the absolute growth rates would be even more pronounced if calculations were compared for fixed values of the supercriticality parameter Δ. Asterisks appearing on the curves in figures 13(a, b) indicate the position along the real x-axis of the saddle point x_s (cf. (3.3)). One also observes from figure 13(b) that the streamwise extent of the absolutely unstable region decreases with increasing r. As a result, evaluation of the integral quantity I in (3.5) will decrease with increasing asymmetry due both to a reduction in Δx_{AU} and in the magnitudes of $\omega_{0_i}(x)$. These effects are shown graphically in figure 14.

The frequency selection criterion discussed previously and defined by (3.3) was compared using the simulations corresponding to the results presented in figures 5

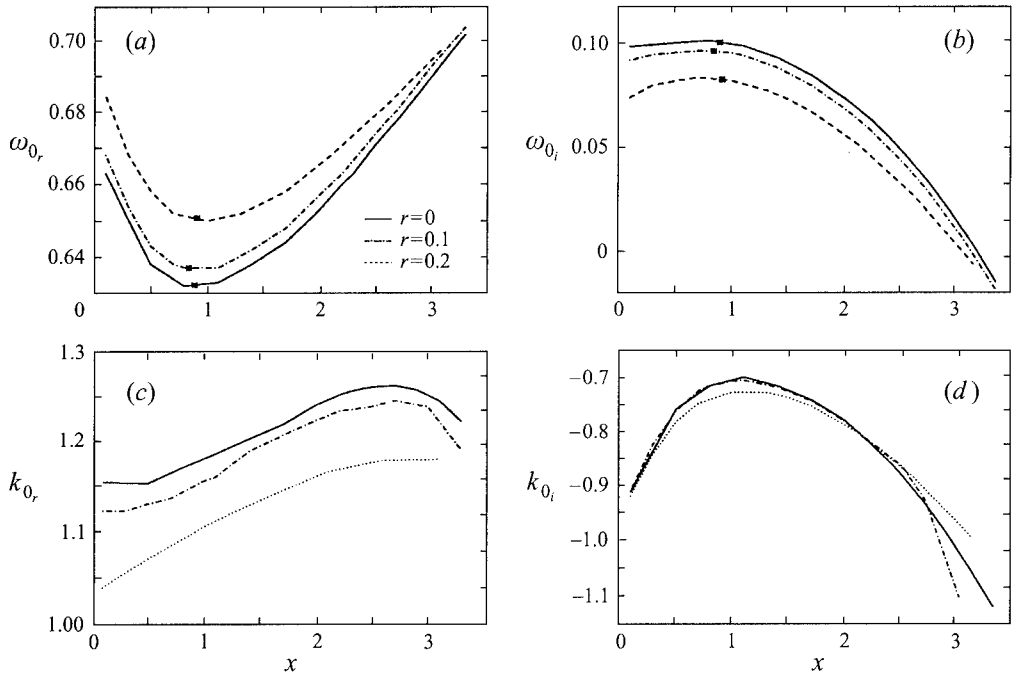

FIGURE 13. The streamwise development of (a, b) the absolute frequency and (c, d) the absolute wavenumber of the asymmetric wake at $Re = 160$.

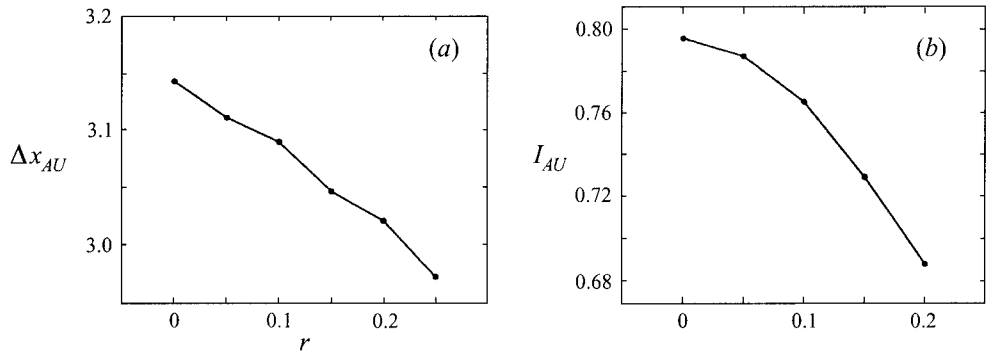

FIGURE 14. (a) The streamwise extent of the region of absolute instability and (b) the size of the absolute instability region as measured by the parameter I_{AU} for the asymmetry wake at $Re = 160$.

and 13. The leading-order asymptotic prediction of the frequency $f_{sp} = (2\pi)^{-1}\omega_{0_r}(x_{sr})$ was evaluated for several velocity ratios. The results are tabulated in table 2. The differences between the observed frequency and that determined by the saddle-point criterion are less than 2% in all cases. The correspondence is quite surprising since there are corrections arising from the non-parallelism of the flow, as defined in the Appendix, and the nonlinear nature of the global mode. It is important to point out that the calculation of f_{sp} already contains some nonlinear contributions, principally those arising from mean flow corrections. Mean flow velocity profiles obtained from a numerical simulation of the full unsteady equations of motion (i.e. vortex shedding active) at a supercritical Reynolds number were used in the local

r	x_{sr}	x_{si}	f	f_{sp}	f_k	f_p
0.00	0.79	0.078	0.1000	0.1006	0.1106	0.1007
0.05	0.74	0.069	0.1004	0.1008	0.1108	0.1007
0.10	0.74	0.066	0.1010	0.1014	0.1103	0.1014
0.15	0.76	0.081	0.1017	0.1023	0.1109	0.1023
0.20	0.81	0.132	0.1026	0.1035	0.1106	0.1038
0.25	0.82	0.128	0.1035	0.1050	0.1108	0.1049

TABLE 2. Saddle-point data and comparison of frequency selection criteria for asymmetric wakes at $Re = 160$.

instability calculations underlying the prediction of f_{sp} reported here. A better test of the theoretical underpinnings would employ velocity profiles from a completely steady simulation (i.e. vortex shedding absent) at the prescribed supercritical Reynolds number. The nonlinear correction from the mean flow correction is expected to be rather weak with a supercriticality parameter $\Delta = 0.33$, but no quantitative test of this exists. One could also consider smaller values of Δ, but transients decay much more slowly as Δ is decreased toward zero.

Alternative *ad hoc* proposals for the frequency selection for a global mode in a spatially developing flow have been advanced by Koch (1985) and by Pierrehumbert (1984). Koch proposed a frequency selection based on the downstream transition point where the flow instability type changes from absolute to convective. This frequency is denoted f_k in table 2. Pierrehumbert proposed that the frequency selected by the global mode corresponds to the real value of the absolute frequency ω_{0_r} at the point where the absolute growth rate ω_{0_i} achieves a maximum. This frequency is denoted by f_p in table 2. The value of f_p will be equal to f_{sp} when the saddle point lies on the real x-axis. However, this implies that the length of the absolutely unstable region is marginally equal to zero. It is evident from figures 13(a, b) that f_p differs, in the present simulations, only slightly from that given by the saddle-point selection criterion. This is because the saddle point is found to lie relatively close to the real x-axis. In any case, the saddle-point selection criterion is found to provide the best estimate. Of course, there is a rigorous basis for the latter criterion.

It is evident from the foregoing results that the strength or vigour of the global mode will decline as the shear or mean flow asymmetry is increased. This rather qualitative remark is made slightly more quantitative by exhibiting in figure 15 the entire global mode for different velocity ratios at a fixed Reynolds number $Re = 320$. In this figure the transverse velocity along the centreline ($y = 0$) of the wake is shown at four different phases of the saturated global mode. We have not attempted a comprehensive scaling of the global mode structure along the lines performed by Goujon-Durand, Jenffer & Wesfreid (1994) for the wake of a circular cylinder. The asymmetry in the present case of the mode about the $y = 0$ axis for $r \neq 0$ is evidence of the asymmetric transverse eigenfunction structure. The eigenfunction amplitude is greater for $y > 0$, where the vorticity is larger and the velocity difference across the shear layer is greater, than it is for $y < 0$. One observes also a clear diminution in the length of the global mode as the shear is increased. Now the streamwise structure of the global mode establishes the amplitude distribution of the synchronized dynamics; it does not reflect the strength of the local vorticity concentrations. The latter is described by the transverse eigenfunction and the magnitude of the phase velocity c relative to the local mean velocity profile $U(y)$ at any location x. For example,

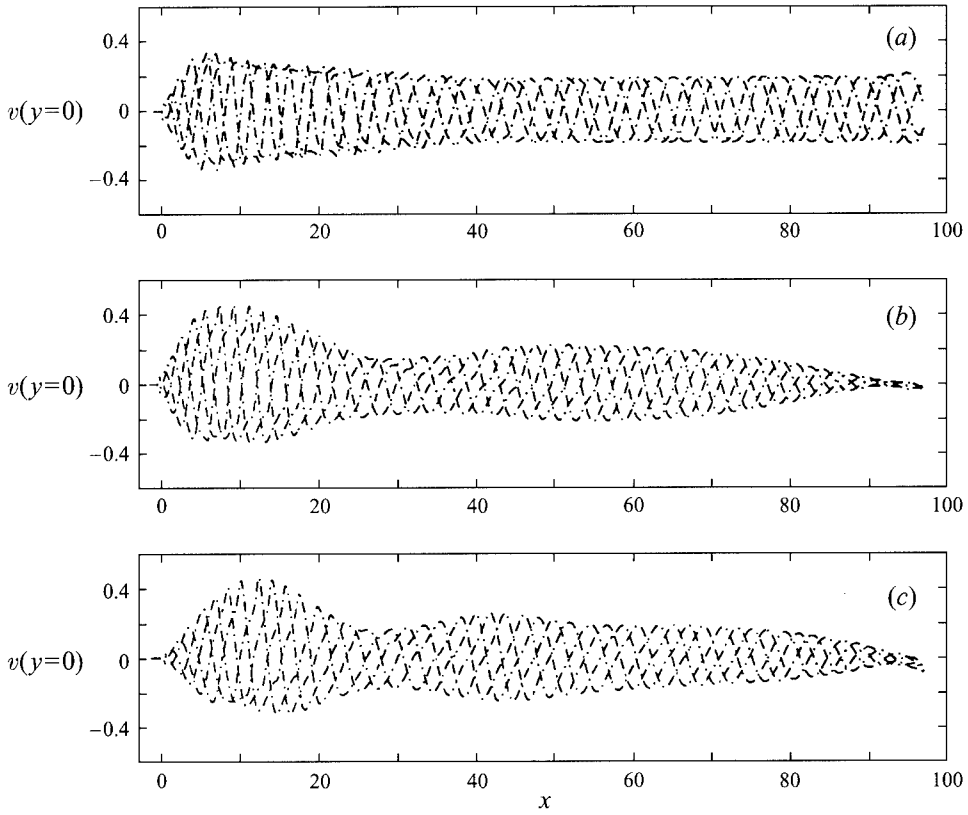

FIGURE 15. The global mode structure at $Re = 320$ for (*a*) $r = 0$, (*b*) $r = 0.1$, (*c*) $r = 0.2$.

if two critical levels exist (i.e. two zeros in the function $U(y) - c$), then there will exist two levels where concentrations of vorticity of opposite sign will form as in the familiar vortex street. However, when the velocity deficit in the wake diminishes with a fixed velocity ratio, only one critical level exists and vorticity concentrations of only one sign, that associated with the shear across the wake, will form. The wake will then transition to a shear layer. It is entirely possible for this transition to occur at some streamwise location within the active domain of the global mode. The vorticity structures in wakes having different velocity ratios are shown in figure 16. The transition from the wake mode to the shear layer mode is especially evident in figure 16(*c*) where a simulation with $r = 0.2$ is shown. The vorticity contours in figure 16 are drawn using the same level values in each of the panels.

Wallace & Redekopp (1992) discussed the transition from a wake mode to a shear layer mode in the context of linear stability theory using wake–shear layer profiles having the velocity deficit and the velocity ratio as parameters. They suggested that a possible measure of where this change in the vorticity distribution from a wake form to a shear layer form occurs might be the streamwise position where the sinuous mode of instability with the maximum spatial growth rate transitions from two critical levels to one critical level. Of course, there is no apparent relation between the most amplified wave according to local linear spatial stability theory and the characteristics of the saturated, supercritical global mode. Nevertheless, this is a well-defined criterion and one that is, at least, quite reasonable for convectively

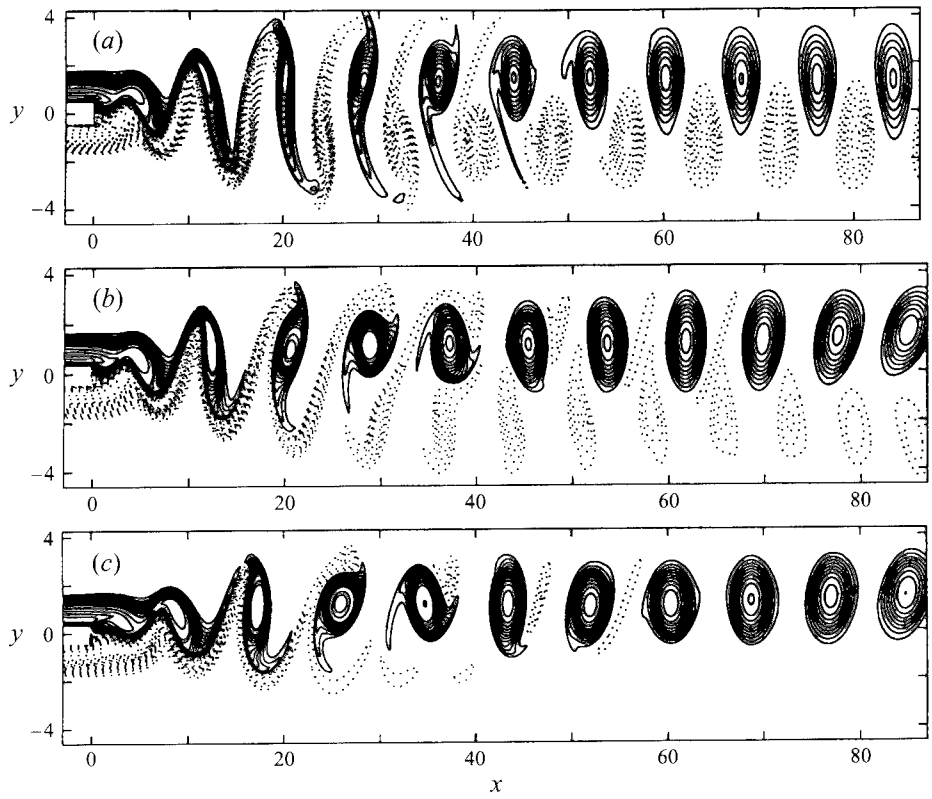

FIGURE 16. Vorticity contours (——, negative vorticity; ·····, positive vorticity) at $Re = 320$ for (*a*) $r = 0$, (*b*) $r = 0.1$, (*c*) $r = 0.2$.

	$Re = 160$	$Re = 320$
$r = 0.1$	15.9	12.8
$r = 0.2$	9.4	6.3

TABLE 3. Transition-point data for x_t based on spatial stability theory.

unstable flows. Computations based on local mean velocity profiles from the present numerical simulations yield the transition points x_t listed in table 3.

5. The effect of suction

A number of different techniques have been proposed for modifying or suppressing the vortex shedding from bluff bodies with the important practical goal of reducing the pressure drag on the body. Monkewitz (1989, 1993) has categorized these approaches to wake control in terms of open-loop and closed-loop control. One of the earliest approaches was that proposed by Roshko (1954) where a thin splitter plate aligned with the free-stream flow was strategically placed along the centreline of the near wake. His experimental results proved quite encouraging. Recently, this approach was explored further through numerical simulations by Grinstein, Boris & Griffin (1991). From the point of view of global modes, one might anticipate that this approach to

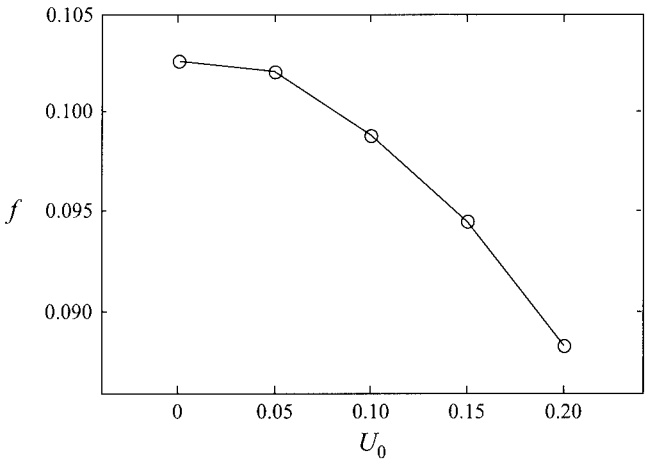

FIGURE 17. The dependence of the vortex shedding frequency of the asymmetric wake ($r = 0.2$) at $Re = 160$ on the trailing-edge suction velocity.

wake modification will be most efficient if the control plate is centred around the location of the saddle point of the absolute frequency (cf. (3.3)). However, we are not aware of any studies to date which have explored this connection with wake control. The control of vortex shedding through this approach is most likely achieved through significant alteration of the local mean velocity profiles with consequent reductions in the local absolute growth rates. The suppression of vortex shedding via insertion of a small control wire placed in the external flow close to the near wake (cf. Strykowski & Sreenivasan 1990) can be rationalized in a similar manner.

In a different approach, base bleed has been shown to be quite effective in reducing the strength of vorticity concentrations and the shedding frequency, even to the extent of suppressing shedding altogether (cf. Wood 1964, 1967; Bearman 1967; Hannemann, Lynn & Strykowski 1986; Hannemann & Oertel 1989; and Schumm *et al.* 1994). Since the region of absolute instability in the near wake exerts a dominant influence on the spatio–temporal dynamics of the wake, it seems clear that the use of blowing or suction from the base of the forebody can be used to alter local stability properties and, thereby, provide a mechanism for wake control or flow modification. In the earlier numerical experiment of Hannemann & Oertel (1989) on a symmetric wake, uniform blowing from the base was applied and a critical value was found for which vortex shedding was suppressed. From a global mode point of view, the velocity deficit in the near-wake profiles was reduced through base bleed rendering the flow less absolutely unstable and, eventually, decreasing the amplification of the global mode to negative values.

In the present study the effect of suction from the base region is investigated. In this case the velocity deficit near the base is expected to be deepened leaving the local flow more absolutely unstable. However, the application of suction should pull the near-wake saddle point of the time-averaged streamlines closer to the base, thereby decreasing the spatial extent of the region of absolute instability. Since the destabilization of a global mode requires that some integral measure of the absolute growth rate over the absolutely unstable region exceeds a critical value (like that proposed in (3.5)), there is an interesting competition occurring and the possible suppression of vortex shedding via suction is worth exploring.

A series of numerical simulations was performed with uniform suction across the

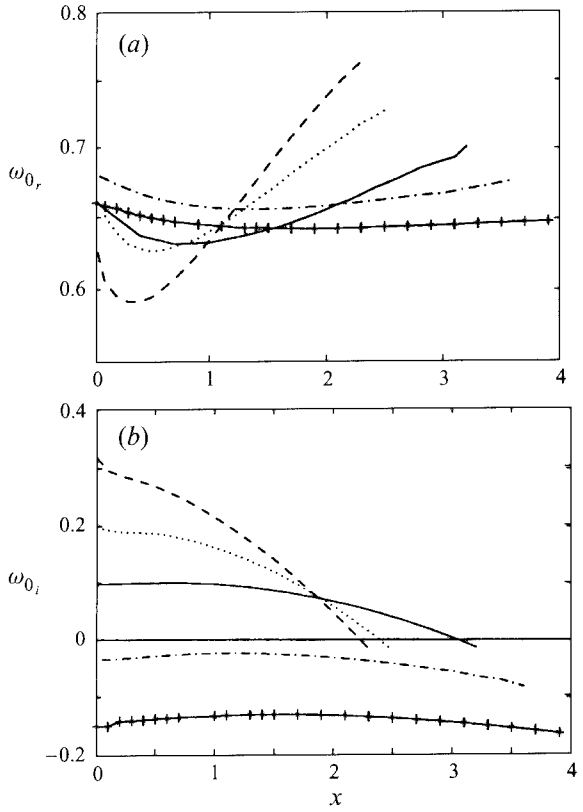

FIGURE 18. (*a*) The real absolute frequency and (*b*) the absolute growth rate of the asymmetric wake ($r = 0.2$) at $Re = 160$ without suction or blowing (—, $U_0 = 0$), subject to blowing (–+–+–+–+, $U_0 = -0.2$; ·····, $U_0 = -0.1$), and subject to suction (· · · · · $U_0 = 0.1$; - - - - -, $U_0 = 0.2$).

base of the rectangular forebody to define the response of the wake to this technique for control. The first case considered was that of a sheared wake with $r = 0.2$ and $Re = 160$. As suction was increased gradually, the wake shedding frequency declined continuously until vortex shedding was abruptly suppressed at a suction velocity of $U_0 = 0.22$ and a completely steady wake flow appeared. The variation of the Strouhal number with suction velocity is shown in figure 17. The distribution of the absolute frequency was computed for cases with uniform suction or blowing. Results are shown in figure 18. One observes that the absolute growth rates increase with increasing suction in the very near-wake region, but that the streamwise extent of absolute instability is continuously shortened and the position of maximum absolute growth rate moves upstream, even to the trailing edge of the body. At the same time the minimum value of the frequency $\omega_{0_r}(x)$ decreases in magnitude consistent with figure 17, and the position of the minimum moves upstream.

Calculations of the location of the saddle point of $\omega_0(x)$ were not made for all the cases with suction because the location of the branch point of the dispersion relation, required for the evaluation of $\omega_0(x)$, became very difficult for mean velocity profiles near $x = 0$ where the shear layers in the wake became very thin. Nevertheless, it appears that this saddle point is very near, if not at, the trailing edge as the suction approaches its critical value for suppression of all global modes. Calculations of the saddle point x_s of $\omega_0(x)$ for low values of the suction velocity in a wake with

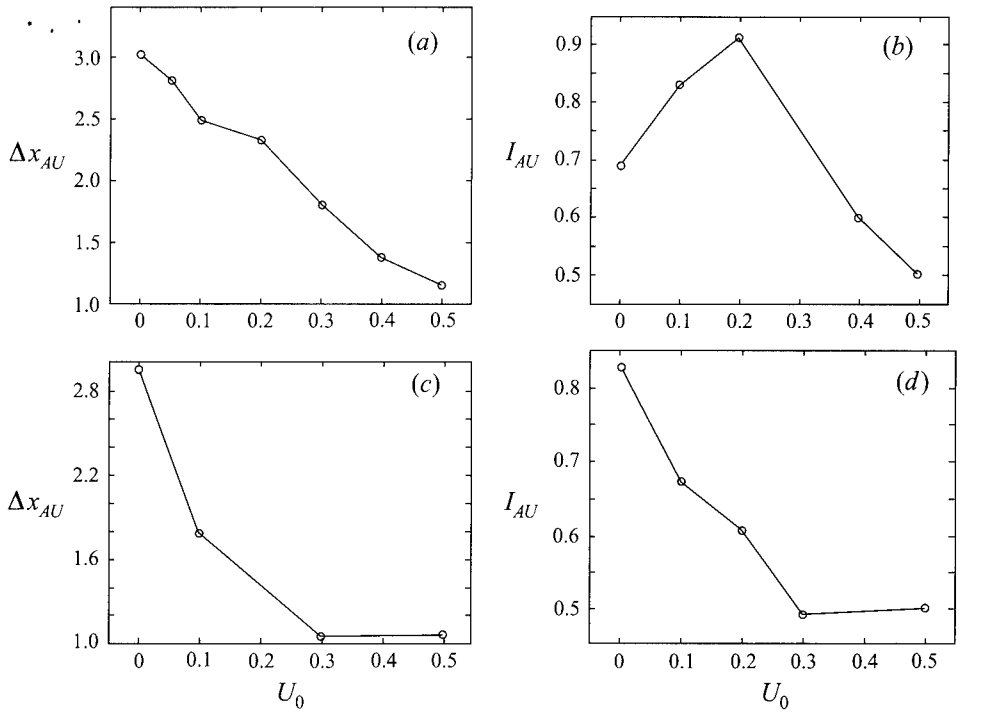

FIGURE 19. (*a*) The streamwise extent of the region of absolute instability and (*b*) the size of the absolute instability region as measured by the parameter I_{AU} for the asymmetric wake ($r = 0.2$) at $Re = 160$ and (*c*, *d*) likewise at $Re = 320$.

$r = 0.2$ and $Re = 160$ are given in table 4, together with the frequencies determined by the different selection criteria. The frequency prediction based on the saddle-point criterion without regard for the boundary condition imposed on the global mode by the presence of the body gives consistently better results.

The discrepancy between the predicted frequency and that observed in the full simulation increases slightly as the suction pulls the position of the saddle point toward the trailing edge. The flow becomes strongly non-parallel as the suction increases and the non-parallel corrections described in the Appendix, although not calculated, are expected to become increasingly important. The location of the downstream end of the absolutely unstable region, together with the value of the integral quantity in (3.5), is displayed in figure 19. The value of the integral I_{AU} becomes more sensitive to the value of $\omega_{0_i}(x)$ near the trailing edge as the suction is increased. At the same time, the evaluation of $\omega_{0_i}(x)$ becomes more difficult in this region. As a consequence, accuracy of the numerical values for I_{AU} is expected to decrease as the suction increases. For example, the initial rise in I_{AU} for $Re = 160$ as the suction increases toward the critical value is believed to be real, but the potential error bounds in the computed values also increase. Nevertheless, there is a clear decline in I_{AU} with increasing suction for $Re = 320$, and at higher suction velocities at $Re = 160$, and the distinct suppression of global dynamics beyond a critical suction velocity is firmly established.

Since base suction is found to be effective in damping all global modes, another sequence of simulations was performed for the purpose of evaluating the critical suction velocity for different flow conditions. The results are shown in figure 20.

U_0	x_{sr}	x_{si}	f	f_{sp}	f_k	f_p
0.00	0.81	0.132	0.1026	0.1035	0.1106	0.1038
0.05	0.64	0.088	0.1020	0.1021	0.1138	0.1025
0.10	0.47	0.079	0.0988	0.1000	0.1148	0.1038
0.15	0.38	0.111	0.0945	0.0979	0.1159	0.1050
0.20	0.33	0.148	0.0884	0.0956	0.1206	0.1019

TABLE 4. Saddle-point data and comparison of frequency selection criteria for asymmetric wakes with suction: $r = 0.2$, $Re = 160$.

In figure 20(a) the critical suction velocity is shown as a function of the Reynolds number at a fixed value of the velocity ratio $r = 0.2$. It is apparent that the value of $U_{0,crit}$ is approaching an asymptotic value as the Reynolds number increases. This is consistent with the experimental work of Leu & Ho (1993) where a critical suction velocity of approximately 0.5 is reported for a symmetric wake at $Re = 2000$. In their study the maximum absolute growth rate in the wake without suction was near 0.1, which is similar to the values we find here. However, the region of absolute instability extends to $x \simeq 4$ in their study while we find $x \simeq 3$. Figure 20(b) shows that the required suction velocity for suppressing global dynamics decreases, at fixed Reynolds number, as the asymmetry of the mean flow increases. The decrease is quite significant and is believed to be only slightly influenced by the fact that the critical Reynolds number for onset of global dynamics decreases slowly with increasing velocity ratio (cf. figure 12).

A very interesting result was observed when the suction equalled or exceeded the critical value for a sheared wake. With supercritical uniform suction from the base in a wake–shear layer, the steady, near-wake flow was observed to be directed (vectored) from the low-speed side toward the high-speed side. To quantify this effect, the saddle point of the near-wake streamline pattern was located in each computed realization for $r = 0.2$, $Re = 160$, and different applied suction velocities. When the suction is below critical and the global mode is active, the streamline pattern for the time-averaged flow was computed. When the suction is supercritical the entire flow is steady and a stationary streamline pattern persists. The angle between the x-axis and a line emanating from the origin at the centre of the base and extending through the computed saddle-point location was measured for each realization. The results are exhibited in figure 21. It is clear that a fairly abrupt symmetry-breaking is possible, but only when all global modes are suppressed. These ideas are pursued in a more comprehensive way in Hammond & Redekopp (1996) where the symmetry-breaking bifurcation is more abrupt at higher Reynolds numbers and deflection angles approaching 30° in each direction are shown to be possible by selective variations in the distribution of the suction velocity across the base. Before ending this section, however, we point out that the concepts associated with global mode dynamics are pivotal to the understanding of this vectored response and its initiation.

6. Conclusions

Numerical simulations, performed in conjunction with local instability calculations, have been performed for the purpose of validating the concept of a global mode in relation to the vortex shedding state. A global mode is a streamwise eigenmode characterized by a discrete frequency which synchronizes the dynamics over large

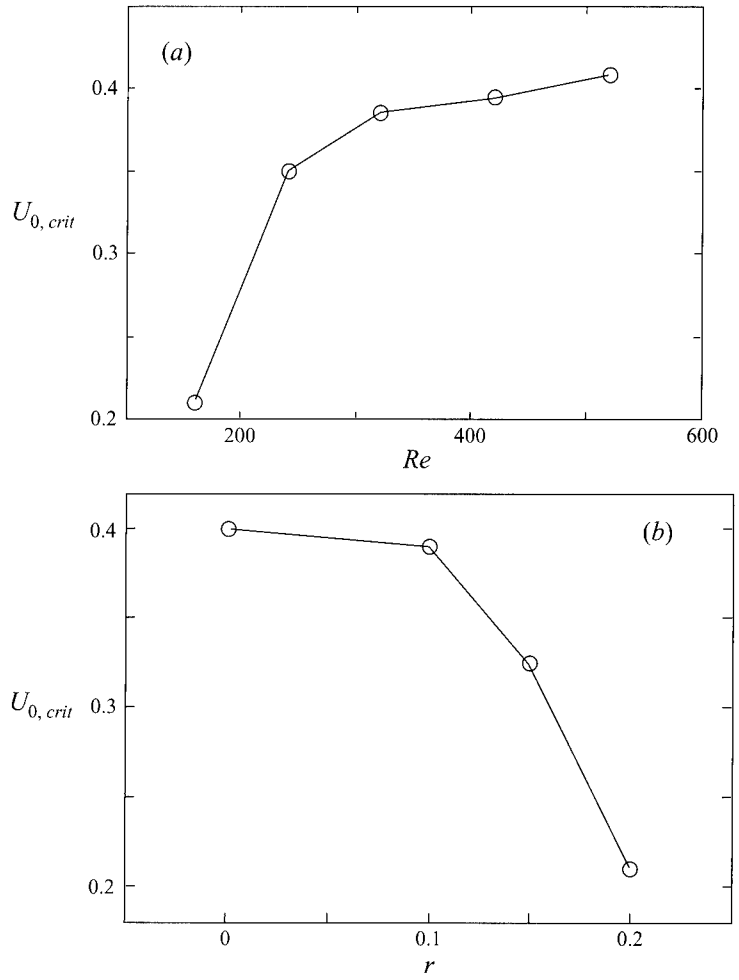

FIGURE 20. The critical suction velocity (*a*) versus Reynolds number at $r = 0.2$ and (*b*) versus velocity ratio at $Re = 160$.

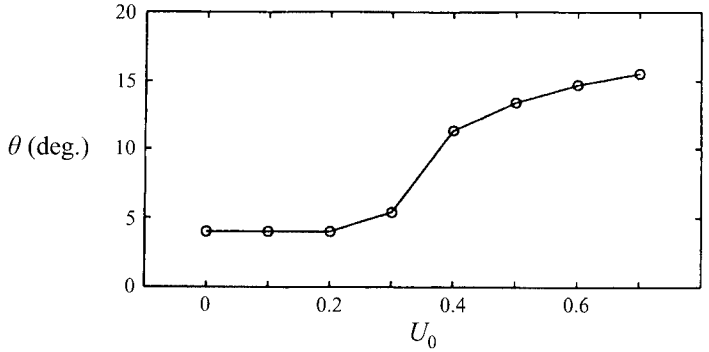

FIGURE 21. The angle of the vectored flow at $Re = 160$ and $r = 0.2$ and its dependence on the trailing-edge suction velocity U_0.

streamwise extents. As described here for the wake of a flow over a rectangular forebody, the gravest global mode is destabilized by a supercritical Hopf bifurcation leading to spontaneous onset of vortex shedding. It has been demonstrated definitively that the normalized Landau coefficient for the local structure of the global Hopf bifurcation is a spatially uniform constant in the wake. This was also shown experimentally by Schumm *et al.* (1994). The intimate connection between the appearance of global dynamics via a global Hopf bifurcation and the existence of a pocket of local absolute instability has been clarified. The global mode shape for the symmetric wake has a streamwise structure with a single maximum in the near-wake region which exists downstream of the absolute instability region. This maximum corresponds quite closely to the region where concentrations of vorticity appear and the formation of the familiar vortex street occurs. The global mode of the asymmetric wake formed by the imposition of a persistent shear across the wake exhibits at least two local maxima in the streamwise variation of the amplitude of the global eigenmode. These streamwise modulations become more pronounced as the shear is increased.

The effects of suction, base-bleed, and shear have been studied and found to diminish the strength of the underlying global mode through their effect on the inherent potential of the absolute instability region in the near wake to induce globally coherent, discrete frequency oscillations. Suction has been shown to diminish the streamwise extent of the absolute instability region by pulling the downstream stagnation point in the near wake streamline pattern of the time-averaged flow toward the origin of the wake. Although the absolute growth rates in the near wake increase due to the increased backflow, the overall effect of suction is to reduce the potential of the absolute instability region to stimulate a global instability. When suction is increased beyond some critical value, which depends on the Reynolds number and the velocity ratio, the absolute instability region reduces sufficiently such that global instability criteria are no longer satisfied and the wake becomes steady and stable to, at least, small perturbations. Base bleed also has the effect of reducing the potential of the absolute instability region for global dynamics, primarily by decreasing the magnitude of the growth rates over the domain of absolute instability. The flow subject to supercritical base bleed also becomes steady and stable to perturbations. The influence of shear on the global stability of the flow has also been investigated. An imposed shear across the wake at fixed Reynolds number leads to a reduction in the magnitude of local absolute growth rates as well as a reduction in the streamwise extent of the absolute instability region. It is anticipated that at larger values of the shear, the global instability will be completely suppressed without the application of any control inputs such as base bleed or suction. As long as $r < 1$, the two ambient streams on opposite sides of the wake are co-flowing and the velocity deficit continuously relaxes in the downstream direction as the wake becomes dominated by shear layer type instabilities. Since shear layers do not exhibit global modes when the two streams are co-flowing, we anticipate the suppression of the global instability through the effect of shear alone to occur at some value of the velocity ratio less than unity but greater than the values as high as 0.3 investigated here. We have attempted to describe the potential of the region of absolute instability in a flow to trigger global instability in terms of an integral quantity (3.5). The proposed quantity shows some promise but, at this stage, it is only suggestive of why certain control inputs enhance or inhibit global instability. Further theoretical efforts are needed to offer more definitive criteria.

The saddle-point theory introduced by Chomaz *et al.* (1991), which is the first

rigorous proposal of a frequency selection criterion for a spatially developing flow, has been shown to provide surprisingly accurate frequency predictions. In the case of the symmetric wake at a supercriticality of $(Re - Re_{cr})/Re_{cr} = 0.33$, the saddle-point theory overpredicts the frequency by less than 1%. As the shear is increased and/or the suction velocity is increased, the saddle-point theory provides less accurate frequency predictions because at these conditions the mean flow deviates more severely from the weakly non-parallel, slightly supercritical conditions which were required for this theory. Nevertheless, the saddle-point theory does provide a surprisingly accurate prediction, even beyond the expected range of application.

This work was supported by AFOSR under Contract number F 49620-92-J-0377. Support for much of the computational effort was provided by the San Diego Supercomputer Center. D. H. acknowledges partial support via a Rockwell International Graduate Fellowship. The authors acknowledge several fruitful discussions with P. Huerre.

Appendix

Monkewitz, Huerre & Chomaz (1993, hereinafter referred to as MHC), provided an analysis for the linear correction to the saddle-point frequency selection derived by Chomaz *et al.* (1991) arising from the spatially varying properties of the underlying waveguide. They presented a WKBJ analysis for weakly non-parallel shear flows at high Reynolds numbers. We describe here an application of their asymptotic theory using the spatially developing mean velocity profiles computed in the direct numerical simulation of the symmetric wake flow at $Re = 160$. Specifically, we compute the terms defined in equation (4.14) in MHC. With these terms to hand, the first correction to the global mode frequency based on the linearized saddle-point criterion can be found.

The MHC theory begins with the Rayleigh stability operator applied to the velocity profile $U(y;x_s)$ at the streamwise position x_s of the saddle point of the absolute frequency $\omega_0(x)$,

$$\mathscr{L}\phi_0 \equiv \left\{(kU-\omega)\left(\frac{\partial^2}{\partial y^2}-k^2\right)-kU''\right\}\phi_0 = 0. \tag{A1}$$

Primes are used here to denote differentiation with respect to the cross-stream coordinate y and (ω,k) form the frequency–wavenumber pair (ω_0,k_0) associated with the branch point values at this streamwise-position. Owing to the spatial non-uniformity of the flow, both the eigenfunction and the eigenvalues will change with streamwise position. The relevant corrections to the eigenfunction are represented by writing the streamwise gradient of $\phi_0(y;k,\omega,x)$ as

$$\frac{\partial\phi_0}{\partial x} = -\phi_{1k}\frac{\partial k}{\partial x} - \phi_{1\omega}\frac{\partial\omega}{\partial x} - \phi_{1x}. \tag{A2}$$

The inhomogeneous equations for the indicated functions are as follows:

$$\mathscr{L}\phi_{1k} = \frac{\omega U'' - 2k(kU-\omega)}{kU-\omega}\phi_0; \tag{A3}$$

$$\mathscr{L}\phi_{1\omega} = -\frac{kU''}{kU-\omega}\phi_0; \tag{A4}$$

$$\mathscr{L}\phi_{1x} = k\left\{\frac{kU''}{kU-\omega}\frac{\partial U}{\partial x} - \frac{\partial U''}{\partial x}\right\}\phi_0. \tag{A5}$$

Analysis type	x_s	k_s	ω_s	$c_s = \omega_s/k_s$
Inviscid	$0.917 + 0.34\mathrm{i}$	$1.209 - 0.747\mathrm{i}$	$0.647 + 0.121\mathrm{i}$	$0.343 + 0.311\mathrm{i}$
Viscous	$0.737 + 0.074\mathrm{i}$	$1.166 - 0.705\mathrm{i}$	$0.632 + 0.1003\mathrm{i}$	$0.359 + 0.302\mathrm{i}$

TABLE 5. Comparison of saddle-point data from an inviscid and a viscous analysis.

Eigenfunction	k_0	ω_0	$c_0 = \omega_0/k_0$
ϕ_0	$1.209 - 0.747\mathrm{i}$	$0.639 + 0.123\mathrm{i}$	$0.337 + 0.310\mathrm{i}$
ϕ_{1k}	$1.209 - 0.747\mathrm{i}$	$0.663 + 0.130\mathrm{i}$	$0.349 + 0.323\mathrm{i}$
ϕ_{1x}	$1.209 - 0.747\mathrm{i}$	$0.644 + 0.142\mathrm{i}$	$0.333 + 0.323\mathrm{i}$

TABLE 6. Modified eigenvalue data used for computation of respective eigenfunctions.

The solutions of (A3) and (A5) are needed, according to (4.14) in MHC, to evaluate the respective contributions to the first-order correction to the global mode frequency. The spatial non-uniformity of the mean flow is clearly evident in (A5). In practice, however, the calculation of the indicated derivatives of the mean velocity profile is a potential source of error. These derivatives were evaluated in the present work by using a forward difference formed by data at $(x_{sr} - \Delta x)$ and at x_{sr}, where $\Delta x = 0.1$ according to the nominal grid used in the simulation.

Since the MHC theory takes the Reynolds number to be sufficiently high so that the leading-order, local stability is based on inviscid theory, local stability calculations were made using the Rayleigh equation (A1). With the local dispersive properties known, the saddle point was located following equation (3.4) in the text and the saddle-point values (ω_s, k_s) were computed. These results are compared in table 5 with corresponding calculations based on a viscous, or Orr–Sommerfeld, analysis of the same mean profiles using the base Reynolds number $Re = 160$. The most striking difference is in the location of the saddle point.

Continuing with the inviscid theory and seeking to evaluate the functions ϕ_{1k} and ϕ_{1x}, another point of difficulty is encountered. The evaluation of these functions requires the computed values of the pair (ω, k) obtained from the branch-point calculation of the local dispersion relations at x_{sr}. Since these values are known only imprecisely, the solvability conditions for (A3) and (A5) are not satisfied exactly. As a consequence, application of a shooting algorithm with matching at some interior point is destined to fail. To circumvent this difficulty, we fixed the wavenumber at $k = k_s = k_0(x_s)$ and iterated the frequency (or phase speed c) until the solvability condition was satisfied. Using velocity data along the real line and the refined, or appropriately modified, eigenvalue pair (ω, k), computation of the functions ϕ_{1k} and ϕ_{1x} was completed. Using velocity field data from the simulation with $r = 0$, $Re = 160$ and no suction/blowing (i.e. $U_0 = 0$), the functions shown in figure 22 were obtained. The iterated frequency–wavenumber pairs associated with these eigenfunction computations are listed in table 6. The entry for ϕ_0 has a different frequency and phase speed than that quoted in table 5 for the saddle point because the present results apply along the real line where the velocity profile data are known. Of course, as noted above, we have used the true k at the saddle point which is located 0.34 units above the real line as specified in table 5.

With the eigenfunctions ϕ_0, ϕ_{1k} and ϕ_{1x} to hand, together with data for both the streamwise and transverse components of the mean velocity, the various quadratures

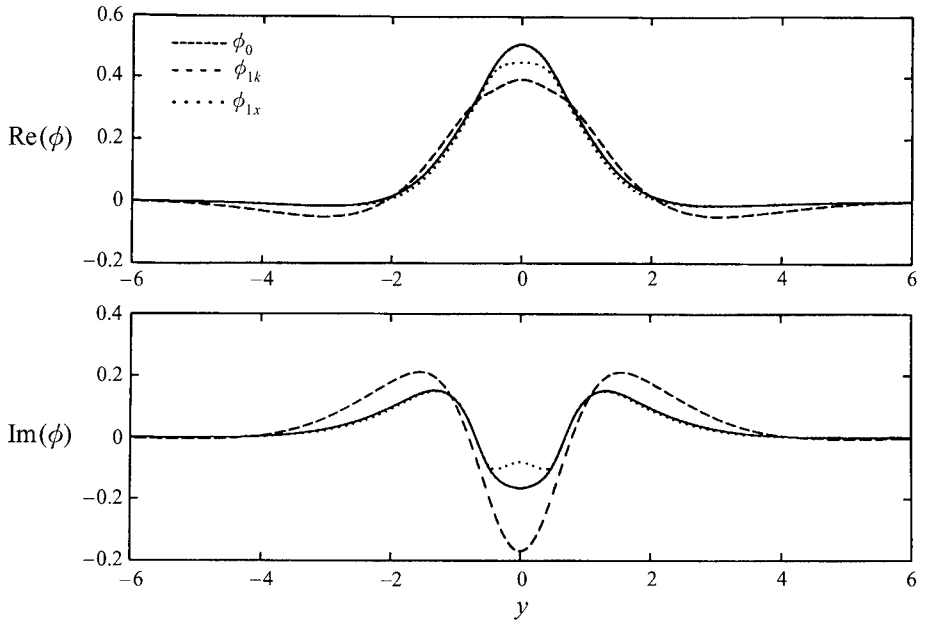

FIGURE 22. Eigenfunctions for $r = U_0 = 0, Re = 160$ used in computing the first correction to the global frequency.

appearing in equations (4.14 *a–d*) in MHC can be evaluated. Following the notation in MHC in exact sequence we obtain the following results:

$$\delta\omega^t = \mathrm{i}\left\{\frac{(0.0735 + 0.0856\mathrm{i}) - (0.4721 - 0.3088\mathrm{i})}{0.1994 - 1.8503\mathrm{i}}\right\} = 0.1902 - 0.2336\mathrm{i}, \tag{A6}$$

$$d^t_{kk} = \frac{2(0.0424 - 0.4791\mathrm{i}) - (0.3226 + 0.5270\mathrm{i})}{0.1994 - 1.8503\mathrm{i}} = 0.7798 - 0.2125\mathrm{i}, \tag{A7}$$

$$d^t_{kx} = \frac{(0.4721 - 0.3088\mathrm{i}) + (0.07796 - 0.05627\mathrm{i}) - (0.04428 + 0.1539\mathrm{i})}{0.1994 - 1.8503\mathrm{i}} = 0.2462 + 0.2468\mathrm{i} \tag{A8}$$

$$d^t_{xx} = \frac{2(0.1025 + 0.1072\mathrm{i}) - (0.00393 + 0.0776\mathrm{i})}{0.1994 - 1.8503\mathrm{i}} = -0.0216 - 0.0298\mathrm{i}. \tag{A9}$$

Each of these expressions has the common denominator, denoted by $L^t_\omega(\phi^t_0)$ in MHC. These results allow calculation of the first correction to the global mode frequency resulting from the linear effects of flow non-uniformity. If the saddle-point location is isolated from boundaries, the complex global mode frequency is given by (6.2) in MHC. If the saddle point is close to a boundary, like the origin of the wake, the complex global mode frequency is given by (6.3) in MHC. The predicted and observed frequencies are summarized in table 7. The first correction, whether the saddle point is essentially isolated from the wake origin or close enough to be influenced by it, has a positive real part and a negative imaginary part. This correction, therefore, yields a Strouhal number that departs even further from the observed value. The correction to the imaginary part of the global frequency is also quite strong (i.e. the growth rate for the global mode). In fact, the correction is so strong for the doubly-infinite case where the saddle point is isolated that the global mode is predicted to be damped. Of

Source	ω_g	Strouhal no. f
Saddle-point criterion (inviscid)	$0.647 + 0.121i$	0.107
Saddle-point criterion (viscous)	$0.632 + 0.1003i$	0.101
Two-term approximation doubly infinite	$0.742 - 0.071i$	0.118
Two-term approximation semi-infinite	$0.734 + 0.027i$	0.116
Observed frequency		0.100

TABLE 7. Comparison of predicted and observed Strouhal numbers.

course, since this is a linear, asymptotic result and the expansion or order parameter ϵ is not necessarily small in the vicinity of the saddle-point location, the next term in the series may have a compensating effect. Furthermore, it is apparent that viscous effects are not insignificant at leading order and are probably underestimated in the two-term approximations calculated here. Also, the numerical simulation is for a supercritical Reynolds number, having a supercriticality parameter $\Delta = 0.33$, and the nonlinear correction to the Strouhal number may in fact be negative, yielding a better correspondence between the prediction and the observation. This is conjecture, of course, but the present results nevertheless seem to provide strong support for the validity of the saddle-point frequency selection criterion. Based on the results presented here, and in the text, it appears that the leading-order prediction using viscous theory for the local stability calculations gives very good agreement with the observed frequencies from the numerical simulations. The agreement on this basis is, in fact, surprising and deserves to be tested further in other settings.

REFERENCES

ALBARÈDE, P. & MONKEWITZ, P. A. 1992 A model for the formation of oblique shedding and 'chevron' patterns in cylinder wakes. *Phys. Fluids* A **4**, 744–756.

BEARMAN, P. W. 1967 The effect of base bleed on the flow behind a two-dimensional model with a blunt trailing edge. *Aero. Q.* **18**, 207–224.

CHOMAZ, J.-M., HUERRE, P. & REDEKOPP, L. G. 1988 Bifurcations to local and global modes in spatially developing flows. *Phys. Rev. Lett.* **60**, 25–28.

CHOMAZ, J.-M., HUERRE, P. & REDEKOPP, L. G. 1990 Effect of nonlinearity and forcing on global modes. In *Proc. Conf. on New Trends in Nonlinear Dynamics and Pattern-Forming Phenomena: The Geometry of Nonequilibrium* (ed. P. Coullet & P. Huerre). NATO ASI Series B: Physics. vol. 237, pp. 259–274. Plenum.

CHOMAZ, J.-M., HUERRE, P. & REDEKOPP, L. G. 1991 A frequency selection criteria in spatially developing flows. *Stud. Appl. Maths* **84**, 119–144.

DAVIS, R. W. & MOORE, E. F. 1982 A numerical study of vortex shedding from rectangles. *J. Fluid Mech.* **116**, 475–506.

DAVIS, R. W., MOORE, E. F. & PURTELL, L. P. 1984 A numerical-experimental study of confined flow around rectangular cylinders. *Phys. Fluids* **27**, 46–59.

EISENLOHR, H. & ECKELMANN, H. 1988 Observations in the laminar wake of a thin flat plate with a blunt trailing edge. *Experimental Heat Transfer, Fluid Mechanics, and Thermodynamics* (ed. R. K. Shau, E. N. Ganić & K. T. Yang). Elsevier.

GOUJON-DURAND, S., JENFFER, P. & WESFREID, J. E. 1994 Downstream evolution of the Benard-von Karman instability. *Phys. Rev.* E **50**, 308–313.

GRINSTEIN, E. F., BORIS, J. P. & GRIFFIN, O. M. 1991 Passive pressure-drag control in a plane wake. *AIAA J.* **29**, 1436–1442.

HAMMOND, D. A. & REDEKOPP, L. G. 1996 Global dynamics and aerodynamic flow vectoring of wakes. Submitted for publication in *J. Fluid Mech.*

HANNEMANN, K., LYNN, T. B. & STRYKOWSKI, P. J. 1986 Experimental investigation of the wake

behind a flat plate with and without the influence of base bleed. *Internal Rep.* IB-221-86-A-26. DFVLR, Goettingen.

HANNEMANN, K. & OERTEL, H. JR. 1989 Numerical simulation of the absolutely and convectively unstable wake. *J. Fluid Mech.* **199**, 55–88.

HUERRE, P. & MONKEWITZ, P. A. 1990 Local and global instabilities in spatially developing flows. *Ann. Rev. Fluid Mech.* **22**, 473–537.

KARNIADAKIS, G. E. & TRIANTAFYLLOU, G. S. 1989 Frequency selection and asymptotic states in laminar wakes. *J. Fluid Mech.* **199**, 441–469.

KARNIADAKIS, G. E. & TRIANTAFYLLOU, G. S. 1992 Three-dimensional dynamics and transition to turbulence in the wake of bluff objects. *J. Fluid Mech.* **238**, 1–30.

KOCH, W. 1985 Local instability characteristics and frequency determination of self-excited wake flows. *J. Sound Vib.* **99**, 53–83.

KOVASZNAY, L. S. G. 1949 Hot-wire investigation of the wake behind cylinders at low Reynolds numbers. *Proc. R. Soc. Lond.* A **198**, 174–190.

LE DIZES, S., HUERRE, P., CHOMAZ, J.-M. & MONKEWITZ, P. A. 1996 Linear global modes in spatially-developing media. *Phil. Trans. R. Soc. Lond.* **354**, 169–212.

LEONARD, B. P. 1979 A stable and accurate convective modelling procedure based on quadratic upstream interpolation. *Comp. Meth. Appl. Mech. Engng.* **19**, 59–98.

LEU, T.-S. & HO, C.-M. 1993 Free shear layer control and its application to fan noise. *AIAA Paper* 93–3242.

MATHIS, C., PROVANSAL, M. & BOYER, L. 1984 The Benard-von Karman instability: an experimental study near the threshold. *J. Phys. Lett.* **45**, 483–491.

MATTINGLY, G. E. & CRIMINALE, W. O. 1972 The stability of an incompressible two-dimensional wake. *J. Fluid Mech.* **51**, 233–272.

MONKEWITZ, P. A. 1988 The absolute and convective nature of instability in two-dimensional wakes at low Reynolds numbers. *Phys. Fluids* **31**, 999–1005.

MONKEWITZ, P. A. 1989 Feedback control of global oscillations in fluid systems. *AIAA Paper* 89–0991.

MONKEWITZ, P. A. 1993 Wake control. In *Bluff-Body Wakes, Dynamics and Instabilities* (ed. H. Eckelmann, J. M. R. Graham, P. Huerre & P. A. Monkewitz), pp. 227–290. Springer.

MONKEWITZ, P. A., HUERRE, P. & CHOMAZ, J.-M. 1993 Global linear stability analysis of weakly non-parallel shear flows. *J. Fluid Mech.* **251**, 1–20 (referred to in the Appendix as MHC).

OERTEL, H. JR. 1990 Wakes behind blunt bodies. *Ann. Rev. Fluid Mech.* **22**, 539–564.

PARK, D. S. & REDEKOPP, L. G. 1992 A model for pattern selection in wake flows. *Phys. Fluids* A **4**, 1697–1706.

PIERREHUMBERT, R. T. 1984 Local and global baroclinic instability of zonally varying flow. *J. Atmos. Sci.* **41**, 2141–2162.

PROVANSAL, M., MATHIS, C. & BOYER, L. 1987 Benard-von Karman instability: transient and forced regimes. *J. Fluid Mech.* **182**, 1–22.

ROSHKO, A. 1954 On the drag and shedding frequency of bluff cylinders. *NACA TN* 3169.

SCHUMM, M., BERGER, E. & MONKEWITZ, P. A. 1994 Self-excited oscillations in the wake of two-dimensional bluff bodies and their control. *J. Fluid Mech.* **271**, 17–53.

SREENIVASAN, K. R., STRYKOWSKI, P. J. & OLINGER, D. J. 1986 Hopf bifurcation, Landau equation, and vortex shedding behind circular cylinders. *Proc. Forum on Unsteady Flow Separation* (ed. K. H. Ghia). ASME FED vol. 52.

STRYKOWSKI, P. J. & SREENIVASAN, K. R. 1990 On the formation and suppression of vortex shedding at low Reynolds number. *J. Fluid Mech.* **218**, 71–107.

TRIANTAFYLLOU, G. S., KUPFER, K. & BERS, A. 1987 Absolute instabilities and self-sustained oscillations in the wakes of circular cylinders. *Phys. Rev. Lett.* **59**, 1914–1917.

TRIANTAFYLLOU, G. S., TRIANTAFYLLOU, M. S. & CHRYSSOSTOMIDIS, C. 1986 On the formation of vortex streets behind stationary cylinders. *J. Fluid Mech.* **170**, 461–477.

TRITTON, D. J. 1959 Experiments on the flow past a circular cylinder at low Reynolds numbers. *J. Fluid Mech.* **6**, 547–567.

WALLACE, D. A. & REDEKOPP, L. G. 1991 Linear instability characteristics of wake-shear layers. *Phys. Fluids* A **4**, 189–191.

WILLIAMSON, C. H. K. 1988 Defining a universal and continuous Strouhal-Reynolds number relationship for the laminar vortex shedding of a circular cylinder. *Phys. Fluids* **31**, 2742–2744.

WILLIAMSON, C. H. K. 1989 Oblique and parallel modes of vortex shedding in the wake of a circular cylinder at low Reynolds numbers. *J. Fluid Mech.* **206**, 579–627.

WOOD, C. J. 1964 The effect of base bleed on a periodic wake. *J. R. Aero. Soc.* **68**, 477–482.

WOOD, C. J. 1967 Visualization of an incompressible wake with base bleed. *J. Fluid Mech.* **29**, 259–272.

ZEBIB, A. 1987 Stability of viscous flow past a circular cylinder. *J. Engng Maths* **21**, 155–165.

J. Fluid Mech. (1997), *vol.* 338, *pp.* 231–248

Global dynamics and aerodynamic flow vectoring of wakes

By D. A. HAMMOND AND L. G. REDEKOPP

Department of Aerospace Engineering, University of Southern California, Los Angeles, CA 90089–1191, USA

(Received 25 October 1995 and in revised form 9 August 1996)

A methodology for vectoring the near-wake flow behind a bluff body without any mechanical movement of the physical boundaries of the generating body is described. The sole control input is suction applied at the fixed base of the forebody. Once the suction volume flux exceeds a critical value needed to suppress the global dynamics associated with vortex shedding, local directional control of the near wake can be achieved. The distribution of suction velocities across the base can be varied to obtain proportional directional control. The role of symmetries in stimulating aerodynamic vectoring of a streaming flow is emphasized and illustrated.

1. Introduction

Mechanical flow control devices such as flaps, elevators, etc. are used extensively on aerodynamic surfaces to achieve lift augmentation and attitude control. This class of movable control devices has recently been incorporated at jet exhausts to accomplish thrust vectoring control for rapid, or enhanced, vehicle manoeuverability, including post-stall performance (cf. Ashley 1995). Even though their application in recent years has led to the realization of quite spectacular manoeuvers, the technology often involves a significant weight penalty, because of the actuator hardware, and a low fatigue life because of severe unsteady loading and direct exposure of control surfaces to high-temperature streams. Another limitation is the slow response time arising from inertia inherent in mechanical systems. For these reasons, and others, it is of some interest to identify *aerodynamic* means of vectoring a flow; that is, to identify methodologies where an external or ducted flow can be re-directed entirely by alteration of boundary conditions and without any mechanical movement of surfaces which guide or constrain the flow. The present work describes a strategy for the aerodynamic flow vectoring of the near wake behind a blunt-based forebody. The aerodynamic control is achieved through suction applied in the base region where the two streams on opposite sides of the planar-shaped forebody separate and form the wake.

Several approaches to vectoring of jets by aerodynamic or fluidic means have been proposed and studied. Fluidic logic devices and jet amplifiers use secondary injection to stimulate directional switching, but the response is usually bistable and not proportional. Some devices also employ Coanda attachment of the primary flow in conjunction with secondary transverse jets (cf. Gilbert 1993). A promising alternative approach has recently been proposed and tested by Washington *et al.* (1996). A low-aspect-ratio two-dimensional jet was designed with a contoured 'collar' on each side which extends beyond the jet exit. Suction is applied on either side

of the jet through the gap between the collar and the divergent section of the jet boundary. A counter-current mixing layer is created on the suction side of the jet with the dynamic effect of a pronounced increase in the local entrainment rate when the suction mass flux exceeds a critical value. The response of the jet is to veer toward the collar on the suction side. Significant vectoring angles have been realized (up to 16°) with minimal loss of thrust. A different scheme involving the use of piezoelectric actuators placed along a blunt face of the exit of a two-dimensional jet has been demonstrated by Smith & Glezer (1994). When an actuator on either side is operating, a zero-mass-flux jet is created which interacts with the primary jet in such a way as to 'attract' the primary jet toward the actuator-induced jet. The transverse force responsible for vectoring the primary jet may arise from the formation of a local separation inside the jet near the exit, but the underlying mechanism for vectoring is not completely clear.

The vectoring of a streaming flow, a flow in which the streamlines of the time-averaged state are nearly parallel, implies that the symmetry of the flow is altered by the application, or by the inducement, of a localized force. In mechanical means of flow vectoring this is accomplished through actuators which change the position of control surfaces, thereby constraining the adjacent flow to move along an altered path. In aerodynamic flow vectoring the flow re-direction is achieved through enforcement of altered boundary conditions. Aerodynamic flow vectoring is closely linked to the symmetry properties of the streaming flow and the boundary conditions. If there is any asymmetry in the pre-existing streaming flow, this can be exploited through modified boundary conditions, which may even be applied symmetrically, to induce a symmetry-breaking of the mean flow streamline pattern. On the other hand, if the original flow has a high level of symmetry, asymmetrically applied boundary conditions are required to stimulate a resulting asymmetric flow pattern. Hence, the underlying symmetry of the flow which is to be vectored is an important consideration in designing a strategy for the aerodynamic vectoring of a flow and in defining its potential for vectoring (i.e. the vectoring response in comparison to the control power required to achieve the vectored state). These issues will become apparent in the results which follow.

The vectoring response of a streaming flow also depends on the nature of local instabilities and the existence, or lack thereof, of any global instabilities. Distinctions between local and global instability, and the character of local instabilities, are quite important to the issues of flow control in general and to the problem of flow vectoring in particular. A discussion of these issues and their relation to the receptivity of a flow to localized forcing is presented by Ho & Huerre (1984) and by Huerre & Monkewitz (1990). It is now firmly established that flows whose local instability is of convective type throughout its streamwise development are quite receptive to upstream disturbances. Small upstream disturbances which exploit the natural amplifier of the unstable system can significantly alter the downstream evolution of the flow. This receptivity of the flow to injected disturbances is lost when the flow is locally absolutely unstable. In this case the control input required to achieve significant flow modification is a significant fraction of the energy of the basic flow. Another possible flow scenario is one where the local instability is of mixed type, yet globally stable. An example of such a state is the spatially developing flow behind a two-dimensional bluff body when the Reynolds number is below the critical value for the onset of vortex shedding. At sufficiently low Reynolds numbers, local profiles of the wake are unstable on a quasi-parallel basis but the flow remains steady because of global stability. However, when the Reynolds number exceeds the

critical value and the region of local absolute instability grows to sufficient size, a Hopf bifurcation occurs giving birth to a globally unstable state (on a linear basis) which is subsequently saturated through nonlinear effects (cf. Mathis, Provansal & Boyer 1984; Sreenivasan, Strykowski & Ollinger 1986; Provansal, Mathis & Boyer 1987; and Schumm, Berger & Monkewitz 1994). The resulting vortex-shedding state is definable in terms of a global mode which characterizes the flow over its global extent. The onset of global instability endows the spatially developing flow with a certain 'rigidity' in that efforts to vector the flow by control actions requires a manipulation (or vectoring) of the whole streamwise eigenfunction underlying the global instability. Obviously, the vectoring potential for such flows is very low. If, on the other hand, the global instability can be suppressed through some control action, then the potential for local vectoring of the separating, near-wake flow is expected to increase dramatically. Results presented subsequently are directed toward the validation of this approach in vectoring the near-wake flow behind a bluff body. Preliminary experimental validation of the methodology described here is provided by Leu & Ho (1993), which originated as a companion part of the present study.

The terms global instability, global mode, and vortex-shedding state are used interchangeably throughout the text which follows. The term global mode implies the existence of a streamwise eigenmode which defines the spatial organization in the streamwise direction of the velocity and vorticity fields. This mode has a discrete frequency which defines the temporal character of dynamical quantities at any spatial position in the wake. In this sense a global mode is a mathematical entity, but physical flow quantities are immediately describable in terms of the eigenfunction for the mode. The term global instability refers to the fact that this global mode is linearly unstable. However, the instability sets in via a supercritical Hopf bifurcation and, hence, is saturated by nonlinearity. It is true, however, that any observable equilibrium global mode is a nonlinear entity. The dynamics of an active global mode are manifested physically as a periodic vortex shedding from the bluff body creating the spatially developing wake flow.

The essential features in the approach to aerodynamic flow vectoring of a wake described here can be summarized in three steps. First, the presence of a region of local absolute instability in the spatially developing wake flow can, if the region of absolute instability exceeds a critical size, trigger a global instability. Second, if a global instability is present in a flow, the vectoring potential of that flow is greatly enhanced when control inputs are employed which suppress the global instability. The use of base suction as a means of flow control is effective in suppressing a global instability in a wake through modification of local instability characteristics. Next, one can use asymmetrically applied suction to induce local vectoring control of the globally stable near-wake flow. Suction accentuates asymmetry in the near-wake flow through asymmetrically induced entrainment from the boundary layers on either side of the forebody.

2. Problem definition

We study the planar flow formed by the passage of two parallel streams with independent ambient velocities over a forebody with a rectangular-shaped trailing edge of height b. We choose to make all variables dimensionless using the base height b as the reference length scale and the average velocity U_∞ of the two independent streams as the reference velocity scale. The flow on either side of the forebody consists of uniform ambient flows with (dimensionless) speeds U_1 and U_2 and Blasius

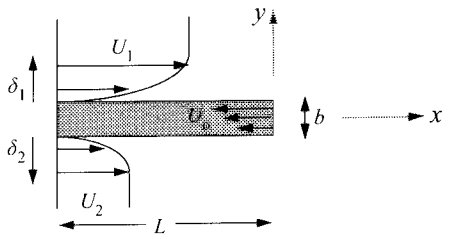

FIGURE 1. Schematic of the flow configuration.

boundary layers with (dimensionless) thickness δ_1 and δ_2, respectively, adjacent to the sides of the forebody. A wake-shear layer develops downstream of the forebody which can be characterized in terms of a Reynolds number R and a velocity ratio r defined as

$$R = \frac{U_\infty b}{\nu}, \quad r = \tfrac{1}{2}(U_1 - U_2), \tag{2.1}$$

where ν is the kinematic viscosity of the homogeneous incompressible fluid. The control variable for the flow is the (dimensionless) suction velocity $U_0(y)$ which is distributed across the base of the forebody. An alternative measure of the control is the suction volume flux (per unit span)

$$q = \int_{-1/2}^{1/2} U_0(y)\,\mathrm{d}y. \tag{2.2}$$

A schematic of the flow configuration is presented in figure 1. We suppose that the high-speed stream is always positioned on the upper side of the forebody as shown in this figure.

The flow described above is studied by direct numerical simulation. The QUICKEST (Quadratic Upwind Interpolation for Convective Kinetics with Estimated Streaming Terms) scheme originated by Leonard (1979) was employed for the solution of the unsteady equations of motion in two space dimensions. The no-slip boundary conditions were applied at the body surface with the exception of the normal velocity along the base which was prescribed by $U_0(y)$. The production version of the code was constructed with a two-level mesh wherein a uniform grid was used in the central strip reaching to the outer edges of each boundary layer and extending from the inlet to the exit of the domain. In the domains outside this strip, and extending to 20 units from the forebody surfaces where the streamwise velocity component was set equal to the ambient velocity, the grid in the transverse direction was stretched by a factor of 8% per interval. The inlet flow consisting of uniform streams with boundary layers at the forebody surfaces was prescribed at a position upstream of the base. At the downstream end of the computational domain, which was nominally positioned at 20 units downstream of the base, convective outflow boundary conditions were applied. Further details of the numerical approach and its validation are described in Hammond & Redekopp (1996).

The results presented herein are limited to low Reynolds numbers in the interest of performing simulations covering a reasonable range of the parameter space with limited computer resources. Furthermore, existing calculations for cylinder wakes show that three-dimensional effects appear for Reynolds numbers exceeding about $(4.3 \pm 0.1)R_{crit}$. The critical Reynolds number for the onset of vortex shedding for sheared wakes behind a rectangular-based forebody is shown in figure 2. Hence, the

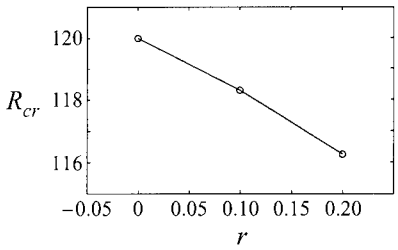

FIGURE 2. The critical Reynolds number for the onset of vortex shedding in the wake-shear layer behind a rectangular-based forebody with $\delta = 1.2$.

highest Reynolds number used in the simulations reported here is $R = 520$ and the grid spacing in the central strip of the computational domain was $\Delta x = \Delta y = 0.1$. This choice of grid also limits the range of inlet boundary layer thickness, an independent parameter in the present formulation, which can be realistically specified. Calculations are reported for boundary layer thicknesses in the range $0.6 < \delta_{1,2} < 1.2$, which translates into displacement thicknesses δ^* in the range $0.2 < \delta^*_{1,2} < 0.4$. Grid refinement studies suggest that the selected grid parameters yield results for global parameters such as the shedding frequency which are accurate to a few percent.

3. Relevant global dynamics

Before discussing simulations of the development of the sheared wake flow with base suction, some relevant results relating to the global dynamics of the flow in the absence of any applied control are reviewed. The definitive establishment of these results, together with a more amplified discussion and reference to related work, can be found in Hammond & Redekopp (1996).

The onset of vortex shedding (or, equivalently, the destabilization of the least-damped global mode) is intimately connected to the existence of a region of local absolute instability in the near-wake region of the spatially developing flow field (cf. Chomaz, Huerre & Redekopp 1988, 1991). In particular, the destabilization of the gravest global mode depends on some integral measure of the absolute growth rate over the region where it is positive. Furthermore, the existence of a locally absolutely unstable flow is related to the form of the velocity profile (principally, the wake deficit and, to some extent, the thickness of the two layers of vorticity comprising the wake profile). The latter result is perhaps most clearly demonstrated by Monkewitz (1988) where the character of the instability for a family of wake profiles is examined. Hence, any control input which modifies the shape of the velocity profiles, and thereby changes the distribution of local growth rates, can exert an influence on the global dynamics of the wake. In particular, suction can exert an influence in two competing ways. First, it will increase the velocity deficit at a fixed position in the near wake leading to enhanced absolute instabilities at that position. On the other hand, suction will tend to pull the saddle point of the time-averaged streamline pattern (i.e. the spatial extent of the near wake) closer to the base, thereby decreasing the streamwise extent of the region of local absolute instability. These two effects are illustrated in figure 3 where local absolute growth rates $\omega_{0_i}(x)$ (i.e. the temporal growth rate of a wavenumber having vanishing group velocity) and the position x_{AU} where $\omega_{0_i}(x_{AU}) = 0$ are plotted for different values of the uniformly

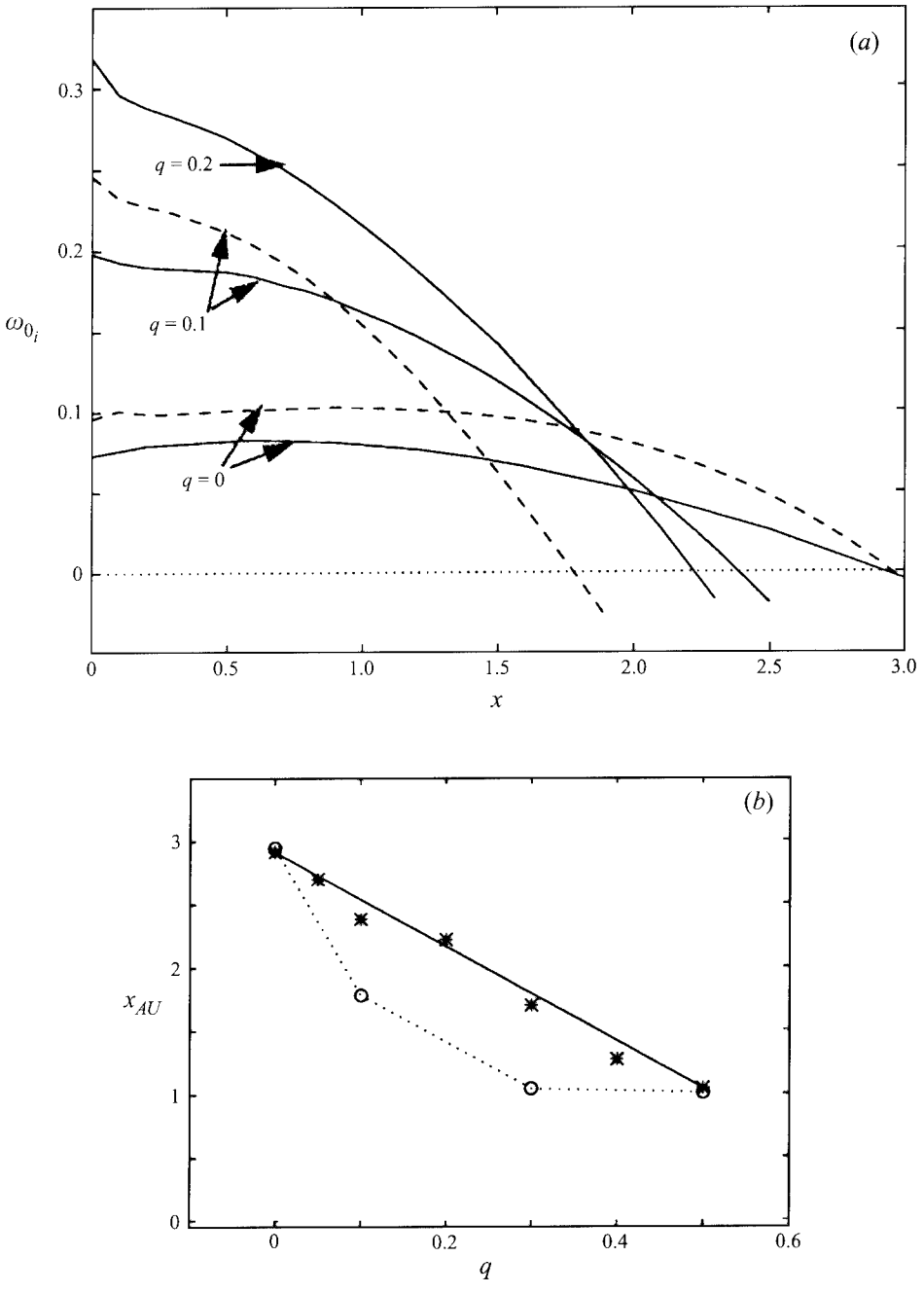

FIGURE 3. (*a*) The absolute growth rate and (*b*) streamwise length x_{AU} of the absolutely unstable region: —, $R = 160$; - - - (*a*), ····· (*b*), $R = 320$.

distributed suction velocity in a sheared wake with $r = 0.2$ at two different Reynolds numbers. The results were obtained from numerical simulations based on the same problem and algorithm described above plus the use of an Orr–Sommerfeld solver using computed local mean velocity profiles. The two effects of suction are evident in

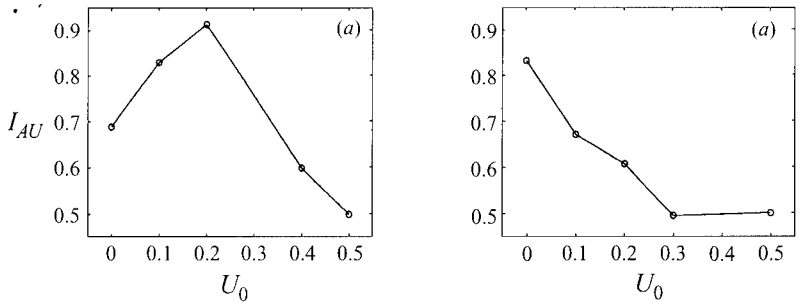

FIGURE 4. The variation of the integral parameter I_{AU} with suction velocity for the asymmetric wake with $r = 0.2$. (*a*) $R = 160$; (*b*) $R = 320$.

the figure and are clearly competing, at least insofar as the suppression of an active global mode is concerned.

Chomaz, Huerre & Redekopp (1990) conjectured that the quantity

$$I_{AU} = \int_0^{x_{AU}} (\omega_{0_i}(x))^{1/2} \mathrm{d}x \tag{3.1}$$

should exceed some critical value for the destabilization of the gravest global mode. No firm theoretical basis exists for the use of this quantity, but some global measure of $\omega_{0_i}(x)$ is believed to define the onset of global dynamics. The quantity defined in (3.1) is, at least, consistent with the model problems considered by Chomaz *et al.* (1988). Evaluation of I_{AU} for a wake with $r = 0.2$ at two Reynolds numbers is shown in figure 4 for cases where a uniform suction velocity is applied across the base. The boundary layer thicknesses in each case were fixed at $\delta_1 = \delta_2 = 1.2$. The sensitive evaluation of mean velocity profiles and values of ω_{0_i} very near the base, especially at higher suction velocities, introduces some uncertainty in computed values of I_{AU}, but the results shown in figure 4 are believed to be accurate to at least 0.025. The non-monotonic variation of I_{AU} observed in figure 4(*a*) arises from the competition described above between increasing values of ω_{0_i} near the base and decreasing values of x_{AU} as the suction flux is progressively enhanced. The increasing values of ω_{0_i} dominate the calculation of I_{AU} initially, but eventually the decreased value of x_{AU}, together with the square-root operation, yields declining values for I_{AU}. Although these computations show that suction applied at the base does not always produce a monotonic decline in I_{AU} as the volume flux is increased, they do suggest that suction may be effective in suppressing global dynamics in wake flows, at least insofar as I_{AU} is representative of the true global instability criterion.

Spurred by the foregoing results, a sequence of simulations was undertaken to identify the critical suction velocity required to suppress vortex shedding when the distribution of suction velocities was uniform across the base. Note that the value of U_0 in this case is equal to the suction volume flux normalized by the average velocity U_∞ and the base height b (cf. equation (2.2)). Results from this sequence of simulations for $\delta_1 = \delta_2 = 1.2$ are summarized in figure 5. For values of U_0 below the curves in each panel of the figure, vortex shedding is active. However, when U_0 exceeds a critical value, say $U_{0_{crit}}$, vortex shedding is always suppressed. It is observed that the value of $U_{0_{crit}}$ is tending to a plateau as the Reynolds number increases and that this critical value decreases quite rapidly, at fixed Reynolds numbers, as the mean flow asymmetry (i.e. shear) increases. These trends are encouraging relative

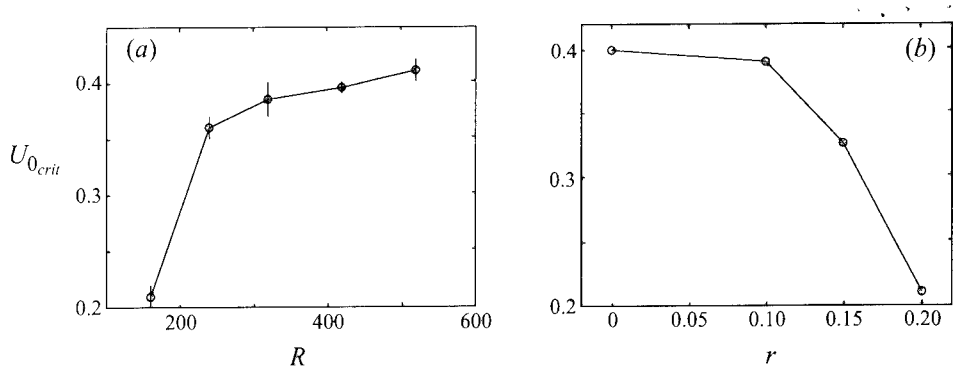

FIGURE 5. The critical suction velocity required to suppress vortex shedding in the wake-shear layer behind a rectangular-based forebody. (*a*) $r = 0.2$; (*b*) $R = 160$.

to scaling the present low-Reynolds-number results to parameter regimes realized in many applications.

We note at this juncture that the effect of the boundary layer thickness on the value of the critical suction velocity enters primarily through the Reynolds number. When global wake parameters such as the shedding frequency are considered, the effect of boundary layers on the forebody is captured by using a Reynolds number defined with a length scale equal to the sum of the base height plus the two displacement thicknesses evaluated at separation. Although we have conducted a range of simulations aimed at validating this effect in relation to $U_{0_{crit}}$ by varying $\delta_{1,2}$ by a factor of two, our results fall within the error band for obtaining $U_{0_{crit}}$. Precise evaluation of $U_{0_{crit}}$ is complicated by the vanishing of the growth rate of the global mode as U_0 approaches $U_{0_{crit}}$. Transients decay very slowly as the growth rate of the global instability tends toward zero and long integration times are required to accurately define the dynamics.

4. Flow vectoring results

It was observed in the course of carrying out the sequence of simulations summarized in figure 5 that the wake flow was entirely steady and the low-speed side was deflected toward the high-speed side as soon as the strength of the suction volume flux exceeded the critical value for the given parameter set. An illustration of this effect is shown in figure 6 where a velocity-vector plot of the steady flow field for $R = 160$, $r = 0.2$ with $\delta_1 = \delta_2 = 1.2$ is exhibited. It is clearly evident that the maximum wake deficit at $x = 3.5$, the last downstream station where the velocity vectors are plotted, is shifted upward toward the high-speed side. The near-wake saddle point of the streamline pattern is also observed to be shifted upward. By comparison, when a similar velocity-vector plot is examined (not shown here) of the time-averaged flow field when U_0 is decreased to a value slightly below $U_{0_{crit}}$ and vortex shedding is active for the same configuration, there is an imperceptible transverse shift in the maximum wake deficit or in the near-wake saddle point from the geometrical centreline of the flow field, even though the mean flow is asymmetric ($r = 0.2$). It is worth noting that the suction distribution was uniform for the simulation shown and, therefore, is not responsible for stimulating any alteration of the symmetry of the flow. The uniform suction entrains a greater volume of fluid from the low-speed stream than from the high-speed stream. The result is a local re-direction of the flow. However,

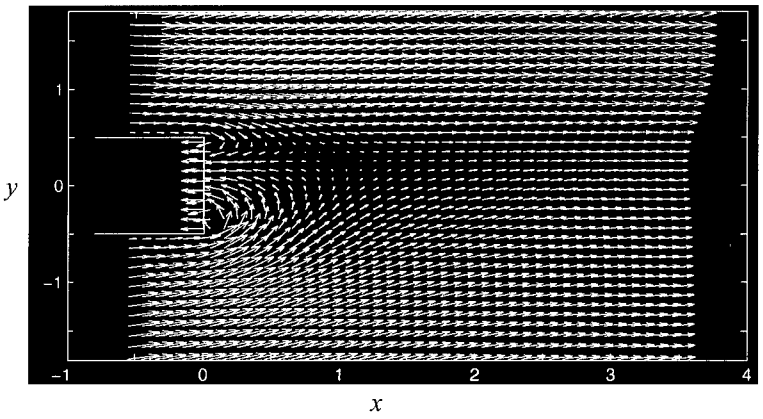

FIGURE 6. The steady velocity field in the near-wake region with supercritical suction distributed uniformly across the entire base ($r = 0.2$, $R = 160$, $q = 0.5$).

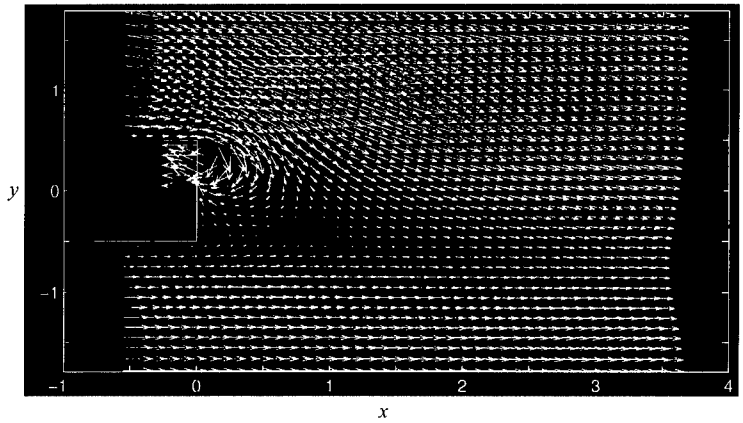

FIGURE 7. The steady velocity field in the near-wake region with supercritical suction distributed uniformly across the half of the base adjacent to the high-speed stream ($r = 0.2$, $R = 160$, $q = 0.5$).

this vectored state can only be achieved after all global modes are suppressed through reduction of the region of absolute instability in the near wake.

With the foregoing results to hand, another simulation was performed with the same flow parameters as in figure 6 and the same supercritical suction volume flux, but the suction was now distributed uniformly over only the (upper) half of the base adjacent to the high-speed side. The response for this asymmetric stimulation is shown in figure 7. One now observes that the suction entrains fluid mostly from the high-speed stream and that the high-speed stream is deflected toward the low-speed side. Consequently, we discover that control of the vectoring *direction* of the near-wake flow can be achieved by selectively varying the *distribution* of the suction volume flux along the base. This vectoring control is possible even in an existing asymmetric flow and with a response in a direction opposite to that selected naturally in the presence of a symmetric stimulation.

The near-wake vectoring described above is accomplished by either exploiting existing asymmetry in the mean flow field or by creating an asymmetry through the control input provided via modified boundary conditions. We emphasize again that the effectiveness of the control input is dependent on the prior suppression of global

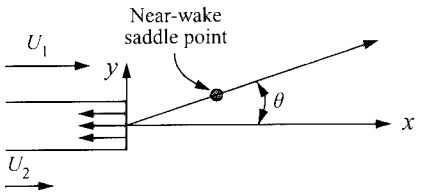

FIGURE 8. Definition of the flow vectoring angle θ.

instabilities in the flow. Now, it has been firmly established that the global dynamics in a wake can be suppressed by the application of either base blowing or suction. The use of base bleed to suppress vortex shedding has been demonstrated by a number of researchers (cf. Wood 1964; Bearman 1967; Hannemann, Lynn & Strykowski 1986; Hannemann & Oertel 1989; and Schumm *et al.* 1994). The results presented here reveal, however, that suction has distinct advantages over blowing when the objective is to vector the near-wake flow field. Base bleed effectively washes out any asymmetry in the near wake and, thereby, dramatically reduces the potential for flow vectoring. On the other hand, base suction accentuates the asymmetries present in the flow, either pre-existing or injected through the control, thereby increasing the potential for flow vectoring. Furthermore, suction can be used to inject additional asymmetries, or overcome existing ones, to obtain selected outcomes.

Quantitative measures of the flow vectoring of the near wake were obtained in two ways: first, by computing the angular displacement of the near-wake saddle points from the wake centreline, specified by the angle θ defined in figure 8; and, second, by computing the normal force per unit span F_N acting on the forebody. The angular displacement θ is evaluated for the time-averaged flow when vortex shedding is active. When vortex shedding is suppressed, the flow is steady and the value of θ is unambiguous. The normal force, assumed to be positive when acting upward (i.e. acting from the low-speed side toward the high-speed side), was evaluated by application of the integral form of the momentum equation using the perimeter of the computation domain as the control surface. Results are presented in terms of the force coefficient

$$C_N = \frac{F_N}{\frac{1}{2}\rho U_\infty^2 b}. \tag{4.1}$$

Another important measure of the flow over the forebody is the base pressure coefficient C_p, which was obtained by evaluating the average of the directly computed pressure distribution along the base of the forebody.

The flow-vectoring angle was computed from a number of simulations performed with different velocity ratios at two different Reynolds numbers when the suction is uniformly distributed across the entire base. Results are exhibited in figure 9. A slight asymmetry, which increases with increasing velocity ratio, is present in the time-averaged flow field at subcritical values of the suction volume flux, especially at the low-Reynolds-number condition. However, as already noted in reference to figure 6, there is a very noticeable vectoring of the low-speed stream upward toward the high-speed stream when the suction flux exceeds the critical value for the suppression of vortex shedding. This is reflected in the increased vectoring angle as the suction flux exceeds the critical value. The onset of flow vectoring is seen to be quite abrupt at the high-Reynolds-number condition. Furthermore, the magnitude of this vectoring increases as the asymmetry of the ambient flow is increased. These curves can be viewed as symmetry-breaking bifurcation diagrams for the flow where the suction

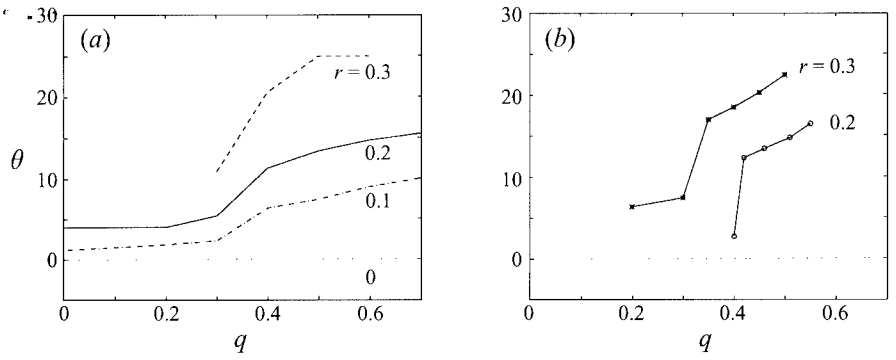

FIGURE 9. The flow vectoring angle as a function of the suction volume flux for suction distributed uniformly across the entire base. (*a*) $R = 160$; (*b*) $R = 520$.

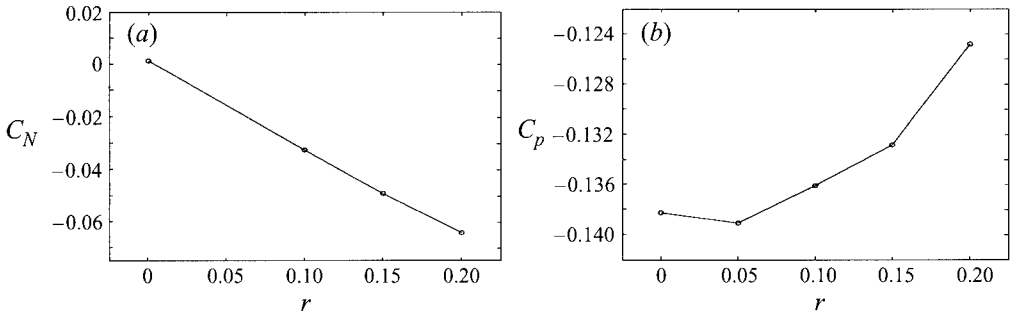

FIGURE 10. The influence of shear on the time-averaged normal force coefficient (*a*) and base pressure coefficient (*b*) in the absence of base suction ($R = 160$).

volume flux serves as the control parameter. Of course, one should recall from figure 5 that the critical value of the control parameter varies for the different conditions (i.e. values of R and r) shown in figure 9.

A more meaningful measure of the vectoring of the flow is obtained by computing the normal force coefficient C_N. In this case it is useful to have some indication of the magnitude of the transverse force acting on the forebody in the presence of an asymmetric flow while vortex shedding is active. The time-averaged values of C_N and C_p were computed for wakes without any suction at $R = 160$, $\delta_1 = \delta_2 = 1.2$ and results are shown in figure 10. One observes that there is a slight negative (downward) force which increases with increasing velocity ratio. This is consistent with the small positive turning angles shown in figure 9 at zero suction. A favourable (for drag purposes) reduction in the base pressure also occurs as the flow asymmetry increases. Although the trend in these results is clear, and the value of C_N at $r = 0$ is indeed close to zero ($C_N(r = 0) = 0.002$), essentially satisfying the symmetry condition, calculations at different conditions were made to define the reliability of reported values of C_N. A worst case value of $C_N = -0.025$ was found for a symmetric wake at $R = 320$. Consequently, reported values of C_N which follow can be accepted with good confidence.

To quantify the potential for vectoring the near wake, two series of simulations were performed for $R = 320$, $\delta_1 = \delta_2 = 1.2$ at a fixed supercritical suction volume flux of $q = 0.5$. In the first series the suction was distributed uniformly over the entire base of the forebody and the near wake was vectored toward the high-speed side. The results

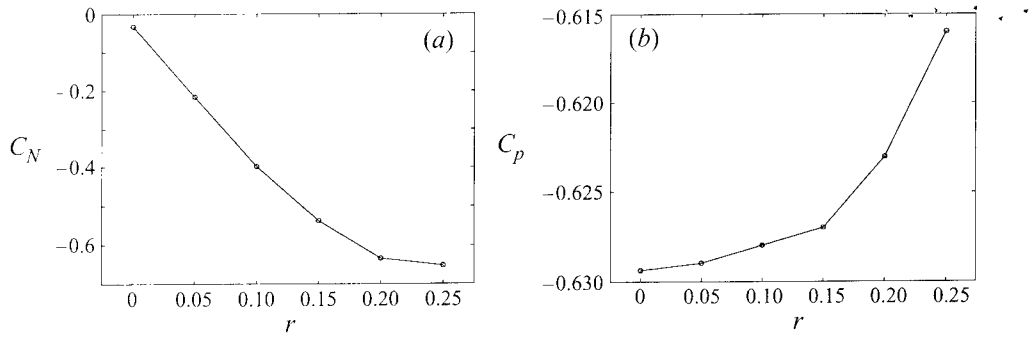

FIGURE 11. The influence of shear on the normal force coefficient (*a*) and base pressure coefficient (*b*) in the steady wake formed with supercritical suction flux with suction distributed uniformly across the base (i.e. vectoring of the low-speed stream toward the high-speed stream). $R = 320$, $q = 0.5$, $\delta_1 = \delta_2 = 1.2$.

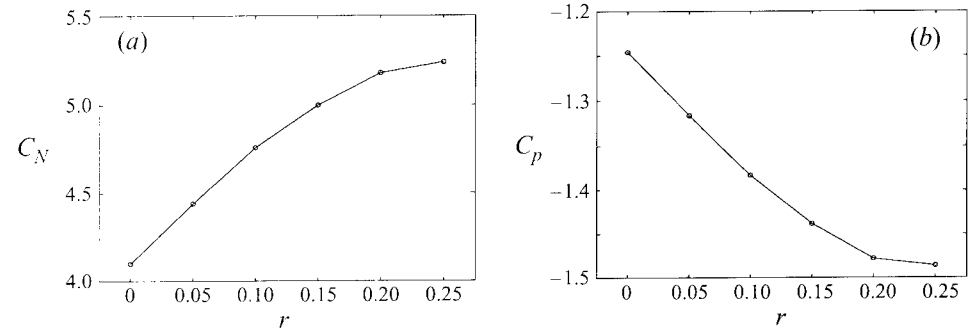

FIGURE 12. As figure 11 but with suction distributed uniformly over only the top half of the base (i.e. vectoring of the high-speed stream toward the low-speed stream). $R = 320$, $q = 0.5$, $\delta_1 = \delta_2 = 1.2$.

for this series are summarized in figure 11. The normal force is an order magnitude larger for the vectored state than it is for the unvectored state shown in figure 10(*a*). The magnitude of the normal force increases monotonically with the velocity ratio with some suggestion that the force may asymptote as the shear increases beyond about $r = 0.3$. The base pressure deficit also decreases in this vectored flow state, but it is still about five times larger than its value in the unvectored state (cf. figure 10*b*.) The suction distribution was confined to the top half of the base, keeping the total volume flux fixed at $q = 0.5$ in the second series of simulations. The results for this series where the high-speed stream is vectored downwards are shown in figure 12. The normal force now acts upward and is an order of magnitude larger than that found in figure 11 for the vectoring of the low-speed stream upward. Of course, the entrainment from the boundary layer on the high-speed side is now much larger than from the boundary layer on the low-speed side because the suction velocities near this side are now twice as large. In both cases, however, it is very evident that the vectored response increases as the inherent asymmetry of the flow increases.

The foregoing results show a decided effect arising from the suction distribution. In fact, they suggest that the suction distribution and volume flux are likely to be important independent parameters in constructing an optimal stimulation to achieve a given vectored state. Of course, practical considerations limit the spectrum of suction distributions that are reasonable. For the purposes of this study, the distributions are

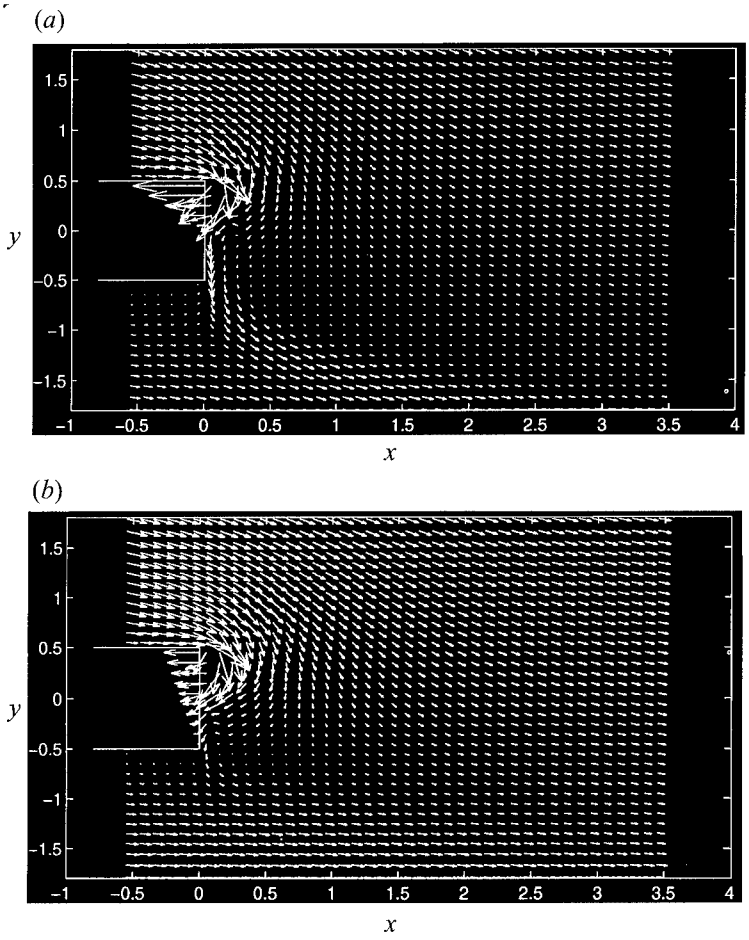

FIGURE 13. The steady velocity field in the near wake of a high-speed vectored flow having a fixed supercritical volume flux arising from different triangular-shaped distributions of suction velocity: (*a*) suction distributed over the top-half of the base; (*b*) suction distributed over the entire base. $R = 320$, $r = 0.2$, $q = 1$, $\delta_1 = \delta_2 = 1.2$.

either uniform, as in the cases already presented, or triangular and extend over either the entire base or are confined to one half of the base adjacent to one of the streams. Two examples involving vectoring of the high-speed stream are shown in figure 13 for a strongly supercritical suction flux of $q = 1.0$. If the suction distribution was uniform across the base, the low-speed stream would be vectored upward. With a triangular distribution skewed toward the high-speed side, the flow is vectored downward toward the low-speed side. If the triangular suction distribution is confined to the top half of the base, a strong downward wall jet is formed along the lower half of the base resulting in a strong vectoring of the high-speed stream. The calculated normal force on the forebody yields $C_N = 7.40$ and $C_N = 6.18$, respectively, for the two flows shown in figures 13(*a*) and 13(*b*). Clearly, the suction distribution can have a very significant role in the vectoring of the near wake.

Further simulations were performed covering a range of supercritical suction fluxes to see if an optimal flux exists for a fixed distribution or if the vectoring response increases monotonically with increased forcing. Since base suction draws fluid princi-

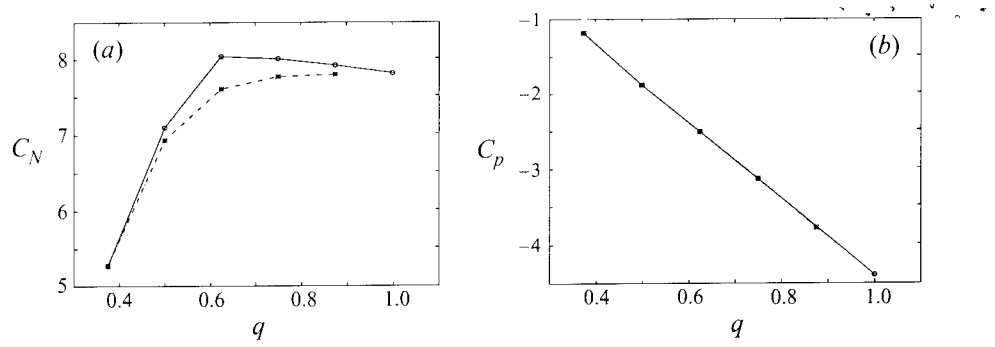

FIGURE 14. The influence of suction volume flux on the normal force coefficient (*a*) and base pressure coefficient (*b*) for a high-speed vectored flow arising from a triangular-shaped suction distribution over the top half of the base. $R = 320$; $r = 0.2$; (——) $\delta_1 = \delta_2 = 1.2$; (— · — · —) $\delta_1 = \delta_2 = 0.9$.

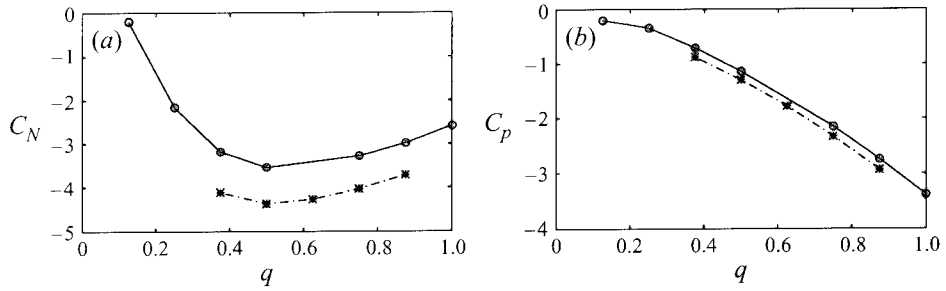

FIGURE 15. As figure 14 but for a low-speed vectored flow arising from a triangular-shaped suction distribution over the lower half of the base.

pally from the boundary layer region, one expects that the boundary layer thickness on the forebody just prior to separation will also have a role in determining the vectoring response. To this end simulations with different inlet boundary layer thicknesses were included in the study. Results for triangular suction distributions over only half the base are shown in figures 14 and 15, respectively, for vectoring the high-speed stream and for vectoring the low-speed stream. In each case, the maximum suction velocity in the distribution is positioned next to the stream to be vectored. Included in the figures are results for two different boundary layer thicknesses. It is apparent that an optimal suction flux exists, at least for the low-speed vectoring shown in figure 15. Examining figure 15 one observes that the optimal flux does not vary significantly with the boundary layer thickness, but the magnitude of the normal force increases as the boundary layer thickness decreases. Interestingly, the high-speed vectoring results in figure 14 show an opposite trend with the boundary layer thickness, although the dependence on the boundary layer thickness is much weaker. One also observes that the base pressure coefficient is essentially independent of the boundary layer thickness for these vectoring results, especially for the case of high-speed-stream vectoring where the differences are indiscernible.

The dependence of such global vectoring quantities as the normal force and the average base pressure on the boundary layer thicknesses was explored further by conducting a set of simulations covering a wider range of δ. For this sequence the suction flux was set at the fixed value $q = 1.0$ which is believed to be significantly removed from the value of q where changes occur because of small departures from the optimal value. Furthermore, a triangular distribution of suction covering the

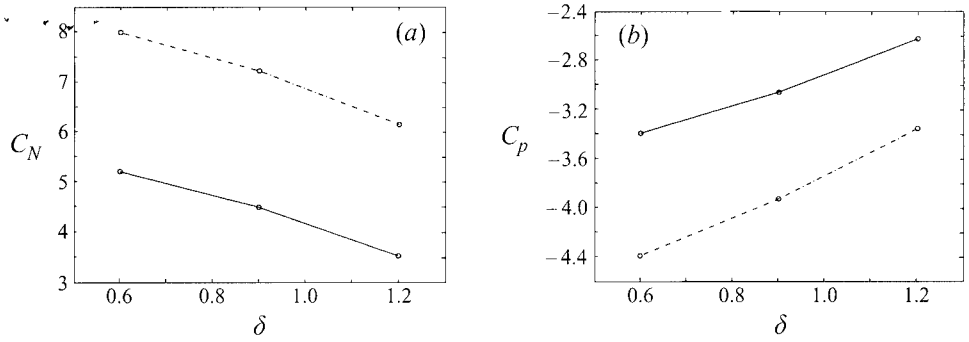

FIGURE 16. Variation of the normal force coefficient (*a*) and base pressure coefficient (*b*) with suction volume flux for a high-speed vectored flow with a triangular-shaped suction distribution extending across the entire base. $R = 320$; $q = 1$; ——, $r = 0$; — · — · — $r = 0.2$.

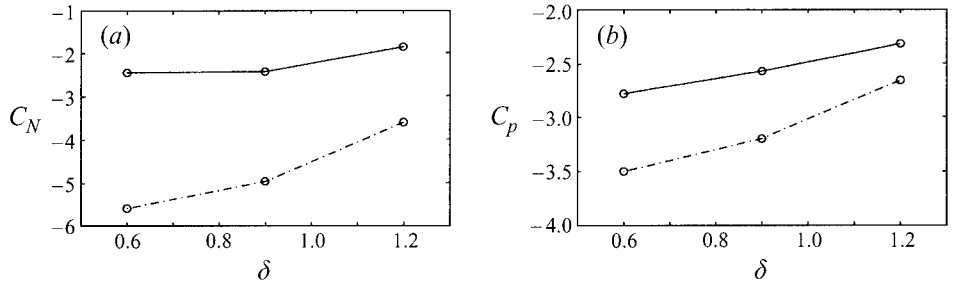

FIGURE 17. As figure 16 but for a low-speed vectored flow with a triangular-shaped suction distribution extending across the entire base.

entire base of the forebody was employed to avoid extremes in the asymmetry of the control effect. With the maximum suction occurring near the top of the base, the results for vectoring the high-speed stream downward shown in figure 16 are obtained. When the triangular distribution is inverted, the vectoring occurs in the opposite direction yielding the results exhibited in figure 17. Results are shown in both figures for a symmetric wake ($r = 0$) and an asymmetric wake with a velocity ratio of $r = 0.2$. Clear trends with δ are found in each case and the opposing variations noted earlier in figures 14 and 15 do not persist. The vectoring response measured in terms of the magnitude of the normal force is now seen to increase, at fixed suction flux and distribution, as the boundary layer thickness decreases. One might argue that the suction volume flux required to achieve a given vectored response (e.g. the normal force) might be related to the displacement effect in the boundary layer of the stream to be vectored. This would imply that the effect of the boundary layer thickness should be evaluated for conditions where the volume flux normalized by the ambient-stream speed and the displacement thickness is held constant. However, this normalization of the suction volume flux cannot account completely for the effect of the boundary layer thickness when an optimal volume flux exists such as shown in figure 15. Consequently, we conclude that there is a decided effect of the boundary layer thickness on the vectoring response arising from a given stimulation which is distinct from its contribution to the specification of the critical suction flux required to suppress vortex shedding (i.e. through the length scale used in the Reynolds number).

The results shown in figures 16 and 17 serve to emphasize a point which has been

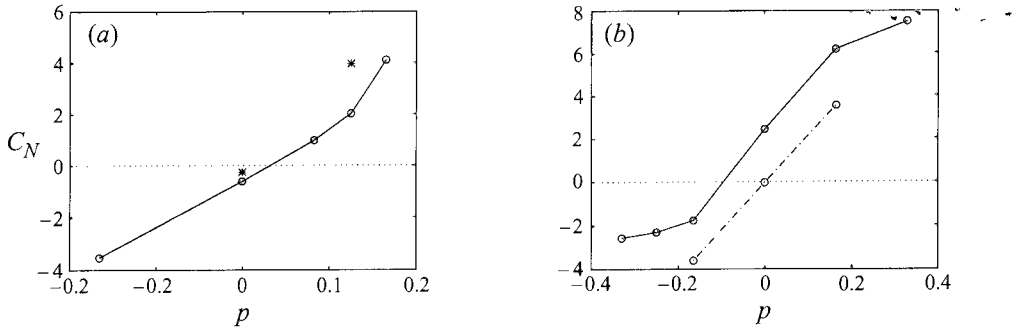

FIGURE 18. Variation of the normal force coefficient with the suction distribution asymmetry parameter p when the suction volume flux exceeds the critical value. (a) The effect of Reynolds number for an asymmetric base flow with $r = 0.2$ and a suction volume flux $q = 0.5$ (—, $R = 160$; *, $R = 320$). (b) The effect of velocity ratio in a wake with $R = 520$ and a suction volume flux $q = 1.0$. Data points at $p = \pm 0.17$ coincide with results for simulations using $R = 320$ and $q = 1$.

alluded to previously. It is evident that an asymmetric suction distribution is effective in vectoring an otherwise symmetric flow and that the response is amplified by an existing asymmetry within the essentially parallel flow. If a flow is entirely symmetric, some asymmetry must be injected through the flow control procedure in order to stimulate a vectoring of the flow. If the flow possesses an inherent asymmetry, it can be vectored by an appropriate symmetric stimulation, but the response can be amplified by the injection of further asymmetry through the flow control stimulus. The symmetry of the basic flow and the control are important elements in aerodynamic vectoring. Of course, the effectiveness of any procedure to stimulate an aerodynamic vectoring of a near-wake flow, however, only becomes operative (or, as a minimum, is greatly enhanced) when all global instabilities are suppressed.

In many applications it is desirable to have proportional control. Since the onset of a vectoring response appears quite abruptly as the suction volume flux exceeds the critical value needed to damp out any global instability, proportional control can be realized by varying the suction distribution. That is, one can use symmetry effects to achieve the desired control response. This is illustrated in figure 18 where results are presented for the response of given flows to a varying distribution of suction. The abscissa p in both parts of the figure is the first moment of the suction distribution

$$p = \int_{-1/2}^{1/2} y U_0(y) \mathrm{d}y. \tag{4.2}$$

The results are obtained from a sequence of simulations with a fixed supercritical value of the suction volume flux and using only a linear variation of $U_0(y)$. Positive values of p have the highest suction velocity on the high-speed side and negative values have the strongest suction next to the low-speed side. A clear proportional response can be realized through variation of the control parameter p, holding all other flow parameters (i.e. q, r and R) fixed. Further control of the response can be obtained by simultaneously varying the magnitude of the suction flux q. In figure 18(a) the suction volume flux is $q = 0.5$ and the results are for an asymmetric wake with $r = 0.2$ at two Reynolds numbers. Since the basic flow is also asymmetric, the normal force vanishes for a positive value of p. Figure 18(b) presents results for both symmetric and asymmetric wakes with $q = 1.0$. At this higher value of q the normal force is

shifted upward (to higher values) at fixed asymmetry of the suction distribution. The reversal in response relative to the symmetric suction distribution point $p = 0$ occurs because, as already evident in figures 14 and 15, there exists an optimal volume flux for a given suction distribution. The saturation of the response at higher values of $|p|$ is also believed to arise from the fact that $|C_N|$ is more strongly peaked around the optimal value of q as $|p|$ increases. Clearly, an optimal performance map could be constructed by varying q at fixed p, but the results presented here are sufficient to establish the character of the vectoring response as a function of the key parameters.

5. Summary

A methodology has been found whereby selective control of the flow direction in the near wake behind a bluff body can be realized. The approach is completely devoid of any mechanical motion of physical surfaces or boundaries which define the flow domain and, therefore, can be legitimately termed a technique for *aerodynamic vectoring* of the flow. The input which is used to stimulate and control the vectored response involves distributed suction applied in the base region of the forebody. The volume flux which is removed through the base must, if measurable vectoring of the near wake is to be realized, exceed the well-defined critical value required to suppress any global dynamics manifested by vortex shedding. When a global mode is active in a flow, it endows that flow with a 'structural rigidity' determined by the underlying streamwise eigenfunction. Such a flow is quite resistive to any modification of local boundary conditions, regardless of their symmetry or asymmetry. However, when all global modes are damped, the local flow in the near-wake region can be readily and selectively re-directed. The directional response can be controlled through the spatial distribution of suction velocities along the base and derives from differential entrainment from the boundary layers on either side of the forebody. Wake bleed or blowing from the base can also be used to suppress vortex shedding, but this means of suppression of global dynamics tends to wash-out existing asymmetry possessed by the mean flow. Suction, on the other hand, accentuates any existing asymmetry resident in the mean flow. Furthermore, an asymmetric distribution of suction can be employed in an otherwise symmetric flow to create a radically asymmetric, or vectored, response. The results presented here suggest that an optimal suction flux exists whereby one can achieve a maximal vectoring of the near wake for a given suction distribution and ambient flow state. Also, those distributions of suction velocity which preferentially entrain fluid from the boundary layer on a given side of the base region will be most effective for the vectoring of the stream on that side of the wake.

The suction volume fluxes required to realize suppression of global dynamics and the onset of flow vectoring in the present study appear relatively large when compared to values commonly used in boundary layer control applications. Of course the goals in the respective cases are quite different. In boundary layer control, no global redirection of the flow is intended and no significant changes in the normal force are realized. Applications of the results presented here might include the development of an aerodynamic flap behind an airfoil section having a blunt trailing edge, or the thrust vectoring of a two-dimensional jet in co-flow where the jet lips are blunt-based. In the latter case, the near wakes behind the blunt-based lips at the jet exit would be vectored in concert; that is, a suction distribution leading to a vectoring of the low-speed co-flow stream toward the high-speed jet flow would be applied at one lip and a distribution leading to a vectoring of the high-speed jet stream toward the

lower-speed co-flow stream would be applied on the other side. Some preliminary simulations aimed at exploring these ideas show promise, albeit the Reynolds numbers in studies to date are quite low.

This work was supported by AFOSR under Contract numbers F49620-92-J-0377 and F49620-94-1-0358. Computer resources provided by the San Diego Supercomputer Center were used in obtaining a substantial portion of the results presented here. D. H. acknowledges partial support from a Rockwell International Graduate Fellowship.

REFERENCES

ASHLEY, S. 1995 Thrust vectoring: a new angle to air superiority. *Mech. Engng* **117**, 58–64.

BEARMAN, P. W. 1967 The effect of base bleed on the flow behind a two-dimensional model with a blunt trailing edge. *Aero. Q.* **18**, 207–224.

CHOMAZ, J.-M., HUERRE, P. & REDEKOPP, L. G. 1988 Bifurcations to local and global modes in spatially developing flows. *Phys. Rev. Lett.* **60**, 25–28.

CHOMAZ, J.-M., HUERRE, P. & REDEKOPP, L. G. 1990 Effect of nonlinearity and forcing on global modes. In *Proc. Conf. on New Trends in Nonlinear Dynamics and Pattern-Forming Phenomena: The Geometry of Nonequilibrium* (ed. P. Coullet & P. Huerre). NATO ASI Series B, vol 237 pp. 259–274. Plenum.

CHOMAZ, J.-M., HUERRE, P. & REDEKOPP, L. G. 1991 A frequency selection criteria in spatially developing flows. *Stud. Appl. Maths* **84**, 119–144.

GILBERT, B. 1993 Deflection of high speed jet flows using fluidics. *Bull. Am. Phys. Soc.* **38**, 2315.

HAMMOND, D. A. & REDEKOPP, L. G. 1996 Global dynamics of symmetric and asymmetric wakes. *J. Fluid Mech.* **331**, 231–260.

HANNEMAN, K., LYNN, T. B. & STRYKOWSKI, P. J. 1986 Experimental investigation of the wake behind a flat plate with and without the influence of base bleed. *Internal Rep.* IB-221-86-A-26. DFVLR, Goettingen.

HANNEMAN, K. & OERTEL, JR., H. 1989 Numerical simulations of the absolutely and convectively unstable wake. *J. Fluid Mech.* **199**, 55–88.

HO, C.-M. & HUERRE, P. 1984 Perturbed free shear layers. *Ann. Rev Fluid Mech.* **16**, 365–424.

HUERRE, P. & MONKEWITZ, P. A. 1990 Local and global instabilities in spatially developing flows. *Ann. Rev. Fluid Mech.* **22**, 473–537.

LEONARD, B. P. 1979 A stable and accurate convective modelling procedure based on quadratic upstream interpolation. *Comput. Meth. Appl. Mech. Engng.* **19**, 59–98.

LEU, T.-S. & HO, C.-M. 1993 Free shear layer control and its application to fan noise. *AIAA Paper* 93–3242. AIAA Shear Flow Control Conference, Orlando, FL.

MATHIS, C., PROVANSAL, M. & BOYER, L. 1984 The Benard-von Karman instability: an experimental study near the threshold. *J. Phys. Lett.* **45**, 483–491.

MONKEWITZ, P. A. 1988 The absolute and convective nature of instability in two-dimensional wakes at low Reynolds numbers. *Phys. Fluids* **31** No. 5, 999–1005.

PROVANSAL, M., MATHIS, C. & BOYER, L. 1987 Benard–von Karman instability: transient and forced regimes. *J. Fluid Mech.* **182**, 1–22.

SCHUMM, M., BERGER, E. & MONKEWITZ, P. A. 1994 Self-excited oscillations in the wake of two-dimensional bluff bodies and their control. *J. Fluid Mech.* **271**, 17–53.

SMITH, B. L. & GLEZER, A. 1994 Vectoring of a high aspect ratio rectangular air jet using a zero net mass flux control jet. *Bull. Am. Phys. Soc.* **39**, 1994.

SREENIVASAN, K. R., STRYKOWSKI, P. J. & OLINGER, D. J. 1986 Hopf bifurcation, Landau equation, and vortex shedding behind circular cylinders. *Proc. Forum on Unsteady Flow Separation* (ed. K. N. Ghia). ASME FED, vol. 52, pp. 1–13.

WASHINGTON, D. M., ALVI, F. S., STRYKOWSKI, P. J. & KROTHAPALLI, A. 1996 Multi-axis fluidic thrust vector control of a supersonic jet using counterflow. *AIAA J.* **34**, 1734–1736.

WOOD, C. J. 1964 The effect of base bleed on a periodic wake. *J. R. Aeronaut. Soc.* **68**, 477–482.